RSC Advances

REVIEW

View Article Online
View Journal | View Issue

Cite this: *RSC Adv.*, 2021, **11**, 14844

Recent advances in photocatalytic nitrogen fixation: from active sites to ammonia quantification methods

Rong Huang,[ab] Xiaoman Li, *[a] Wanguo Gao,[a] Xu Zhang,[a] Sen Liang*[b] and Min Luo *[a]

Photocatalytic nitrogen fixation has become a hot topic in recent years due to its mild and sustainable advantages. While modifying the photocatalyst to enhance its electron separation, light absorption and nitrogen reduction abilities, the role of the active sites in the catalytic reaction cannot be ignored because the N≡N nitrogen bond is too strong to activate. This review summarizes the recent research on nitrogen fixation, focusing on the active sites for N_2 on the catalyst surface, classifying common active sites, explaining the main role and additional role of the active sites in catalytic reactions, and discussing the methods to increase the number of active sites and their activation ability. Finally, the outlook for future research is presented. It is hoped this review could help researchers understand more about the activation of the nitrogen molecules and lead more efforts into research on nitrogen fixation photocatalysts.

Received 11th December 2020
Accepted 31st March 2021

DOI: 10.1039/d0ra10439f

rsc.li/rsc-advances

1. Introduction

As an important component of nitrogen fertilizers, ammonia (NH_3) is significant for all life on earth. It is also a vital raw material for making chemical products, such as nitric acid and explosives. What's more, NH_3 is an ideal hydrogen storage material with green and high energy hydrogen release capacity. The global ammonia output is about 15 billion tons per year. With economic development and population growth, this number is increasing.[1] At present, the Haber–Bosch process is commonly used in industrial ammonia production. However, the application of the Haber–Bosch process for NH_3 production must be carried out at a pressure higher than 200 bar and a temperature higher than 673 K, and it also needs to consume a large amount of H_2 produced by steam reforming of fossil fuels. About 35% of the world's natural gas and 13% of the world's electric energy are usually consumed in the Haber–Bosch process.[2] Therefore, the catalytic process of NH_3 production without H_2 at ambient pressure and temperature is very necessary for the clean and safe synthesis of NH_3.[3]

The atmosphere contains about 78% nitrogen resources,[4] so if the nitrogen can be used directly under normal temperature and pressure, it will bring great energy saving. Coincidentally, photocatalysis, driven by electrons and protons excited by photons, could promote the reduction of N_2 to produce NH_3 under mild conditions. In 1977, Schrauzer and Guth published their first study on photocatalytic nitrogen fixation. They concluded that nitrogen (N_2) could be reduced to ammonia by Fe doping TiO_2 under ultraviolet radiation. Surprisingly, the energy provided by the sun per hour on the surface of the earth can meet the world's energy needs for a year.[5] Photocatalytic nitrogen fixation has attracted more and more attention.

Photocatalytic nitrogen fixation is a kind of green and pollution-free mild reaction, which does not need high temperature and pressure. It can directly use solar energy to generate electrons and holes and combine with water protons to reduce N_2 to NH_3. The principle of photocatalysis is that the semiconductors absorb photon to generate the holes and electrons driving the oxidation–reduction reaction. When the energy of irradiated light is greater than or equal to the band gap of semiconductor nanoparticles, the electrons in the valence band will be excited to the conduction band, leaving relatively holes on the valence band, thus forming electron–hole pairs. Due to the existence of many defects and dangling bonds in nanomaterials, these defects and dangling bonds might capture electrons or holes and prevent the recombination of electrons and holes. These trapped electrons and holes diffuse to the surface of the particles respectively, resulting in a strong redox potential. Therefore, shown in Fig. 1, photocatalytic reactions generally involve three reactions: light absorption, charge carrier separation and surface reduction.[6]

At present, the research of metal compound catalyst and nonmetal compound catalyst is very hot. The common

[a]*State Key Laboratory of High-efficiency Utilization of Coal and Green Chemical Engineering, School of Chemistry and Chemical Engineering, Ningxia University, Yinchuan, Ningxia, 750021, China. E-mail: martinluomin@163.com; lixm2017@nxu.edu.cn*

[b]*Ningxia Key Laboratory for Photovoltaic Materials, Ningxia University, Yinchuan, Ningxia 750021, China. E-mail: liangsen@nxu.edu.cn*

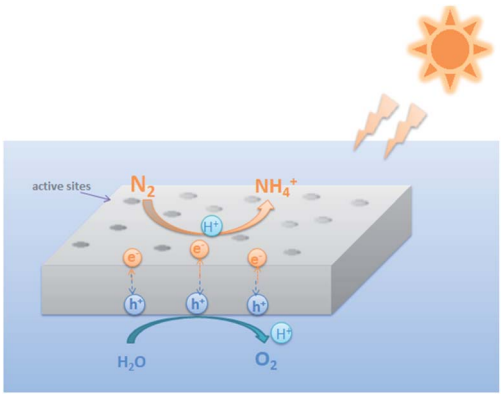

Fig. 1 A simple diagram of photocatalytic nitrogen fixation.

photocatalysts, such as g-C_3N_4,[5,7] TiO_2 [8] and BiOCl,[9] have low nitrogen fixation efficiency because of their light absorption range and charge carrier recombination and other problems. Therefore, in recent years, there have been many studies on the modification of these materials, such as doping,[10] building heterojunction,[11] increasing vacancy[12] and other methods to change the semiconductor band gap,[13] promote photogenerated electron–hole separation,[14] and expand the adsorption of N_2 on the catalyst surface.[15]

Most of the existing reviews are classified from the chemical composition of photocatalyst[16] or from its structural engineering.[2] In this paper, the characteristics of photocatalyst for nitrogen fixation are briefly described, and the classification of photocatalyst is described from active sites on its surface.

2. Principles of photocatalytic nitrogen fixation materials

In the development of photocatalytic nitrogen fixation, the types of catalysts are abundant. Among the metal catalysts, titanium-based catalysts are the most researched materials in the early stage, mainly TiO_2.[17] In recent years, there have been reports of Ti_3C_2 [18] as the catalyst precursor. In addition, iron oxides, metal sulfides,[19] and bismuth oxyhalides (BiOX (X = Cl, Br, I)) are also hot materials for research. Among the non-metallic catalysts, the research on g-C_3N_4 has been the most popular, and its composite materials with precious metals,[20] graphene, black phosphorus,[21] *etc.* have good nitrogen fixation effects. In addition, research on single-atom catalysts[22] and layered double hydroxide (LDH) catalysts[23,24] has gradually increased in recent years. Photoinduced electrons from these semiconductors are used to reduce N_2 to NH_3. The reaction and potential of these semiconductor catalysts to reduce nitrogen to ammonia are shown in the following formula. Under the irradiation of UV visible light, the generated valence band holes can oxidize water (eqn (1)), and conduction band electrons will reduce nitrogen (eqn (2)). NH_3 is finally generated by water and oxygen under light conditions (eqn (3)).[25]

$$2H_2O + 4h^+ \rightarrow O_2 + 4H^+ \text{ (1.23 V } \textit{vs.}\text{ NHE)} \quad (1)$$

$$N_2 + 6H^+ + 6e^- \rightarrow 2NH_3 \text{ (}-0.09\text{ V } \textit{vs.}\text{ NHE)} \quad (2)$$

$$1/2N_2 + 3/2H_2O \rightarrow NH_3 + 3/4O_2 \ (\Delta^0 = 339\text{ kJ mol}^{-1}) \quad (3)$$

How to choose a suitable photocatalytic nitrogen fixation catalyst? On the one hand, it is necessary to consider the common problems of all photocatalysts, as well as the light absorption and carrier transfer. On the other hand, for the nitrogen fixation photocatalyst, the unique features are the adsorption of nitrogen molecules and the desorption of ammonia products.

2.1 Appropriate band gap energy of semiconductor

For photocatalytic nitrogen fixation, the ideal band gap value is close to 2.0 eV, the corresponding light wavelength is less than 620 nm, the value of CB should be less than overpotential of N_2 (-0.092 V *vs.* NHE), and VB level must be greater than the oxidation potential of water (1.23 V *vs.* NHE).[26] Some photocatalysts have insufficient response to visible light because their band gap is too wide or too narrow.[27] In response to this problem, some semiconductor materials have been modified into suitable photocatalysts. Fig. 2 shows the schematic diagrams of the electronic energy bands of several common photocatalysts.

Common modification methods include designing heterojunctions,[18] doping with other elements,[28] changing the structure of nanomaterials, *etc.* These methods can change the band gap of semiconductor materials. For example, Qin, *et al.* prepared Ti_3C_2 nanosheets by etching Ti_3C_2 layered precursor Ti_3AlC_2 (MAX phase), then grown different proportions of 0D $AgInS_2$ nanoparticles *in situ* on the surface of Ti_3C_2 nanosheets, and finally successfully produced different quality Z-scheme heterostructure photocatalyst constructed with 0D $AgInS_2$ nanoparticles and 2D MXene (Ti_3C_2) nanosheets.[18] $AgInS_2$ is a wide band gap semiconductor with a band gap of 1.62 eV, and the band gap of Ti_3C_2 is small, about 0.75 eV. The band gap of the heterostructure AT-30 formed by the two is about 1.00 eV (Fig. 3), and a narrow band gap semiconductor was successfully synthesized. Under visible light irradiation, the photogenerated electrons of $AgInS_2$ are excited and transition from VB to CB, and then transfer to the Ti_3C_2 surface in close contact with $AgInS_2$ to participate in the reduction reaction of nitrogen molecules by the catalyst (Fig. 3d). Its nitrogen fixation yield is 38.8 μmol g^{-1} h^{-1} under visible light irradiation. In addition to building a heterojunction between a wide band gap semiconductor and a narrow band gap material to change the band gap of the composite photocatalyst, some non-metallic atoms can be doped to change the band gap of the compound. Maimaitizi *et al.* synthesized flower-like hierarchical N doped MoS_2 (N-MoS_2) microsphere with one-step solvothermal method.[29] Meantime, photo-ultrasonic reduction method was employed to loaded Pt nanoparticles on the surface of N-MoS_2. It was found that the N doping could narrows the band gap and increase the response range of photocatalyst to visible light. The final yield of nitrogen reduction is 121.2 μmol g_{cat}^{-1} h^{-1}. Also, Wu *et al.* reported compounds containing Bi as photocatalysts.[30] Bismuth

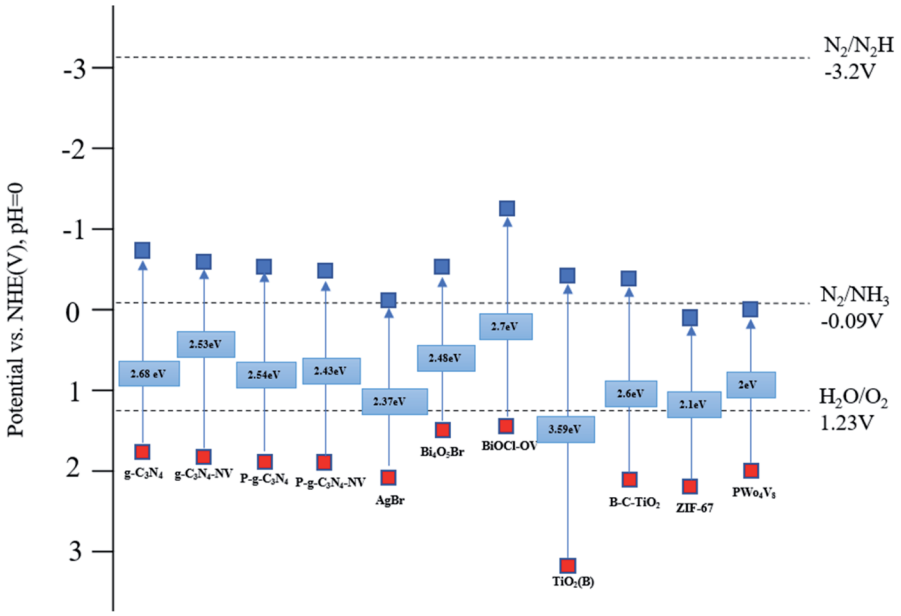

Fig. 2 Schematic diagram of the electronic band structure of several typical semiconductor photocatalytic materials.

chloride microchips with oxygen vacancy were prepared by surfactant assisted solvothermal method by introducing Br to replace Cl in the process of ion exchange, a cavity is formed in Br doped BiOCl-OV (Br-BiOCl-OV) crystal structure. After ion exchange, the Br heteroatom not only reduces the band gap, but also increases the top of the valence band energy level (VB), thereby obtaining a better light trapping ability and provide higher redox potential for N_2 optical fixation. Ammonia production rate increased from 4.1 μmol h^{-1} to 6.3 μmol h^{-1}.

In addition, reducing the size of the crystal structure of photocatalyst is also used to change the band gap. For example, Xue and his colleagues prepared the porous few-layer g-C_3N_4 by simple molecular self-assembly method.[31] Compared with the original g-C_3N_4, the material is ultra-thin and the size is reduced, and its band gap has changed from 2.69 eV to 2.61 eV.

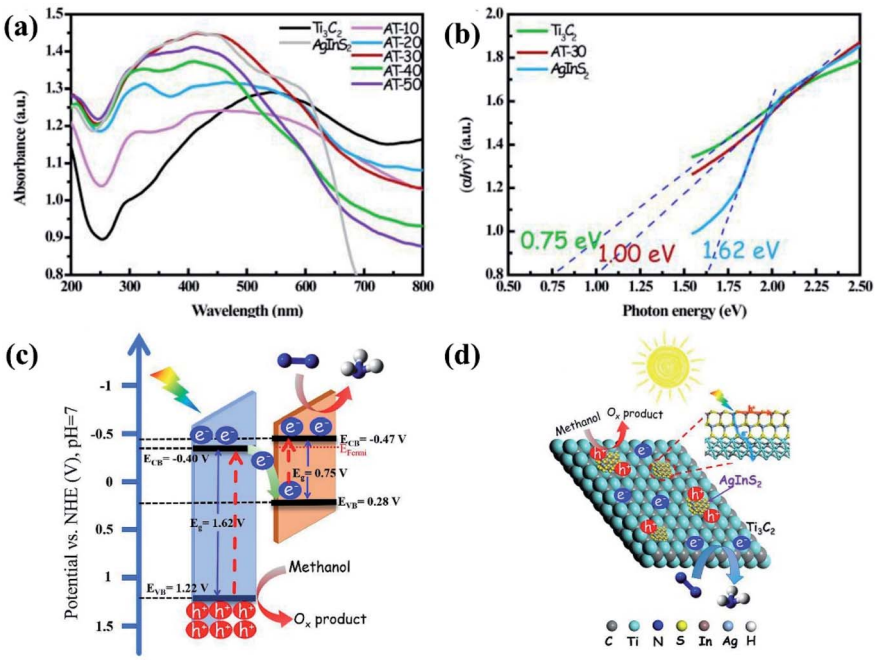

Fig. 3 (a) UV-vis DRS of all the as-prepared samples; (b) Taucs plot of Ti_3C_2, $AgInS_2$ and AT-30 for band gaps; (c) the energy band positions, and (d) scheme for spatial charge separation and transportation during photocatalytic N_2 reduction over $AgInS_2/Ti_3C_2$ nanosheets.[18] Copyright 2019, Elsevier.

2.2 Efficiency of charge separation

Constructing a heterojunction,[32] using a co-catalyst[18] manufacturing surface defects,[33] doping,[34] *etc.* are all effective methods to improve the efficiency of carrier separation (Fig. 4).

Using appropriate methods to increase the surface defects of the material, such as oxygen vacancies, is a common effective means to increase the efficiency of catalyst charge separation. Take the study of Wang *et al.* as an example.[35] As the first discovered and studied photocatalyst, the electron–hole recombination rate of TiO_2 is very high. Wang *et al.* investigated that the core defects in TiO_2 nanotubes containing a lot of charge recombination centers. They used urea, dicyandiamide (DA) and cyanamide as precursors to prepare hydrogen treated TiO_2 (TiO_2–H_2) nanotubes with less oxygen vacancies. Through a series of studies, it is found that the oxygen vacancy in metal oxides has strong fluidity. Because the thermal activation process involves oxygen diffusion and vacancy migration, these defects tend to migrate from the core to the surface after heat treatment. The rearrangement of oxygen vacancy reduces the core defect of TiO_2 as charge composite center and improves the efficiency of charge separation and nitrogen reduction.

The use of promoters to improve the electron transfer efficiency of materials is also a widely used method in recent years. Qiu reported that black phosphorus is used as a co-catalyst for graphite carbon nitride, which increases the number of excited electrons and improves the separation efficiency of carriers by forming C–P covalent bonds.[36] In addition, using graphene as cocatalyst can also improve the separation efficiency of electron hole pairs. According to the works of Fei and others, the hybridization of Bi 6s and O 2p orbitals of Bi_2WO_6 formed the valence band, while the W 5d orbitals composed the conduction band simultaneously.[37] Due of this special band structure, Bi_2WO_6 has become an outstanding visible light catalyst with narrow band width (2.8 eV), which has better chemical properties and stability than the general monolayer catalysts. Compared with graphene nanoribbons and graphene nanosheets, the quantum confinement effect of zero-dimensional graphene quantum dots (GQD) is more obvious and the edge effect is stronger. Fei *et al.* found that the introduction of GQD makes the photogenerated electron–hole pair have higher separation ability (Fig. 5). In the report of Fei *et al.*, the ammonia synthesis rate of GQD/Bi_2WO_6 composites prepared by hydrothermal method under visible light is 241.07 μmol g^{-1}, which is 33.8 times and 8.88 times higher than that of GQD and raw Bi_2WO_6. This good result can be attributed to the effective combination of GQD and Bi_2WO_6. When the nitrogen molecules adsorbed on the surface of the material obtain protons from the solution, it also obtains photoelectrons from the catalyst in time, thereby generating NH_4^+ (Fig. 5c). In this reaction, the carrier separation efficiency of the material is high to ensure that the reaction can have a continuous supply of electrons.

Heterojunction is a widely used method to improve the charge transfer ability of catalysts. Chen *et al.* Constructed the Z-scheme heterojunction of AgBr and $Bi_4O_5Br_2$, and used the silver nanoparticles formed *in situ* after AgBr decomposition as the bridge of charge transfer under illumination to improve the catalytic performance.[32] In addition, doping is a common modification method for photocatalysts. Taking the report of Gao *et al.* in 2019 as an example,[34] they doped metal Zn into δ-Bi_2O_3. Without changing the cubic crystal phase of Bi_2O_3, Zn was successfully placed in the two-dimensional thin δ-Bi_2O_3 material by interstitial doping to help the separation and transfer of photogenerated electrons and holes.

Fig. 4 Methods to improve the efficiency of charge separation of catalyst.

2.3 Chemical adsorption of nitrogen and NH_3

The effective adsorption of nitrogen molecules on the surface of photocatalyst is one of the important conditions for the reduction of nitrogen under light. Many catalysts do not adsorb enough N_2 due to smooth surface[38] or small specific surface area,[39] which results in low catalytic activity.

The surface of the material is exfoliated by chemical method to increase its roughness, which can effectively increase the specific surface area of the catalyst and promote its adsorption of nitrogen molecules. A recent example, edge-rich black phosphorus nanoflakes (eBP NFs) was reported to be successful nitrogen fixation photocatalyst in ambient condition.[21] The eBP NFs synthesized by Bian and his coworkers with chemical etching exfoliation method has rough surface and rich edges, and a large amount of N_2 is chemically adsorbed on the edge of catalyst (Fig. 6). However, although the specific surface area of the material plays an important role in the catalytic reaction, it is more important to increase more chemical adsorption sites than to increase the specific surface area. For instance, $CeCO_3OH$/g-C_3N_4/CeO_2 ternary photocatalyst (2Ce–CN) was synthesized by an *in situ* one-pot hydrothermal method with $CeCl_3$ and (g-C_3N_4) as precursor.[40] It was found that the increase of specific surface area of 2Ce–CN, providing more physical adsorption sites for N_2, and $CeCO_3OH$ in the ternary system provides more Ce^{3+} sites to enhance chemisorption of N_2. In addition, Zhang *et al.* employed high-temperature peeling methods to achieved ultra-thin carbon nitride(g-C_3N_4-V).[41] It's worth noting that the carbon vacancies in g-C_3N_4 extremely promoting the adsorption and activation of dinitrogen molecule, greatly improving the catalytic activity for the defective ultrathin g-C_3N_4-V photocatalyst. This phenomenon proves that

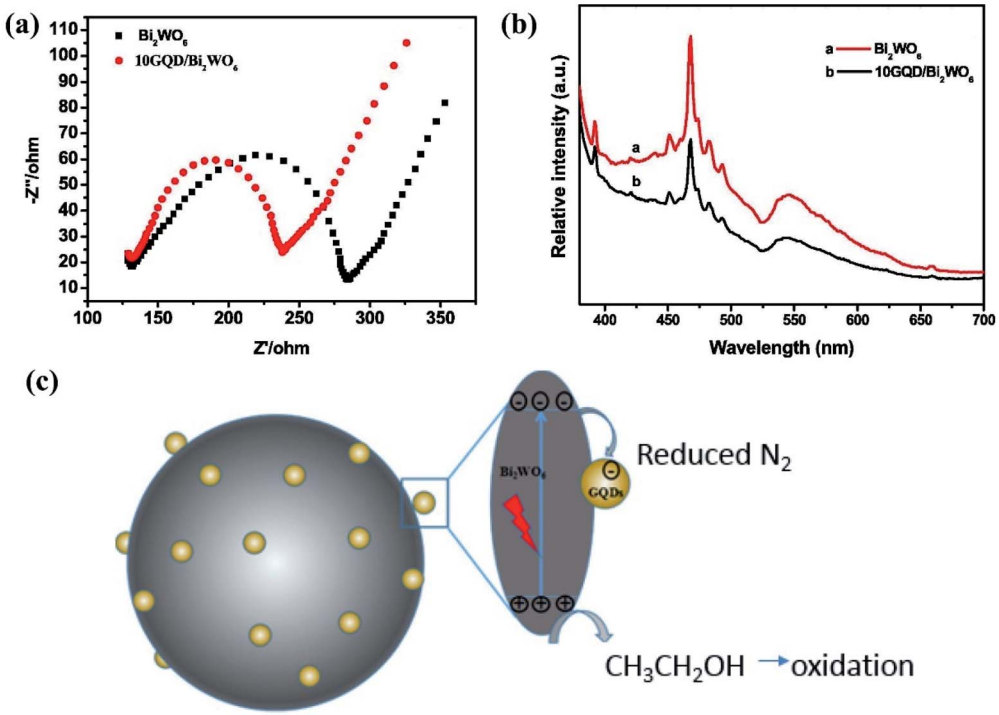

Fig. 5 (a) The electrochemical impedance spectroscopy (EIS) measurements and (b) PL of pure Bi_2WO_6 and 10GQD/Bi_2WO_6 catalysts; (c) schematic of the possible reaction mechanism of photocatalytic nitrogen fixation procedure.[37] Copyright 2019, Elsevier.

the increase of active sites is more important than the increase of specific surface area.

Of course, in photocatalytic nitrogen fixation, it is not enough to only pay attention to the adsorption of nitrogen molecules, but also to the desorption of ammonia. Taking Gao *et al.*'s report in 2021 as an example, after comparing the adsorption energies of different materials for nitrogen and ammonia, they first proposed the influence of the adsorption energy of catalytic product NH_3 on the nitrogen fixation performance of the catalyst.[42] In this report, they tried to improve the catalytic performance by improving the desorption of the product.

Based on the above discussion, it can be concluded that nitrogen reduction reaction photocatalyst must have appropriate band gap to absorb visible light, high separation efficiency of photogenerated electron–hole pair to ensure the continuous reduction reaction and excellent ability to adsorb and activate nitrogen molecules to achieve good catalytic activity.

3. Active sites in nitrogen fixation reactions

The active sites on the surface of photocatalyst are the key to the catalytic reaction, which can not only chemically adsorb N_2, but also establish an effective channel for the transfer of photoexcited carriers from photocatalyst to adsorbed N_2 molecules.[43] According to the recent reports on photocatalysts for nitrogen reduction reaction, the common active sites are vacancy,[44] metallic element,[45,46] *etc.*, which will be described in detail in the next part.

3.1 Vacancies

With more and more photocatalytic nitrogen fixing catalysts being found, increasing the surface defects of the catalysts is an effective way to improve their activity. According to the research of Wang *et al.*, they constructed metal nanocrystals/semiconductor oxide composites with oxygen vacancies (defect sites) as photocatalysts for nitrogen fixation.[47] It was found that metal nanoparticles have small size and special extraction plane effect, which can expose a lot of large coordination unsaturated points as N_2 activation center.[48] At the same time, the surface defect sites are generally used as great nitrogen molecular activation sites, weakening the N≡N triple bond.[49]

Vacancy, a common surface defect, has been found to be the active site, including O,[44,50–53] N,[54–56] C,[41] S,[57] F[58] and other vacancies. Oxygen vacancy refer to the vacancies formed in oxygen-containing compounds where oxygen atoms (oxygen ions) in the crystal lattice break away, resulting in oxygen deficiency. Nitrogen vacancy, that is, the vacancy formed after nitrogen in the crystal lattice of nitrogen-containing compound is separated. Table 1 summarizes the photocatalytic nitrogen fixation activity of the reported catalysts containing different vacancies. It can be clearly found that when the different vacancies are used as active sites, the difference in atmosphere, composite materials, scavengers, *etc.* is different for the improving the capacity of nitrogen fixation of materials.

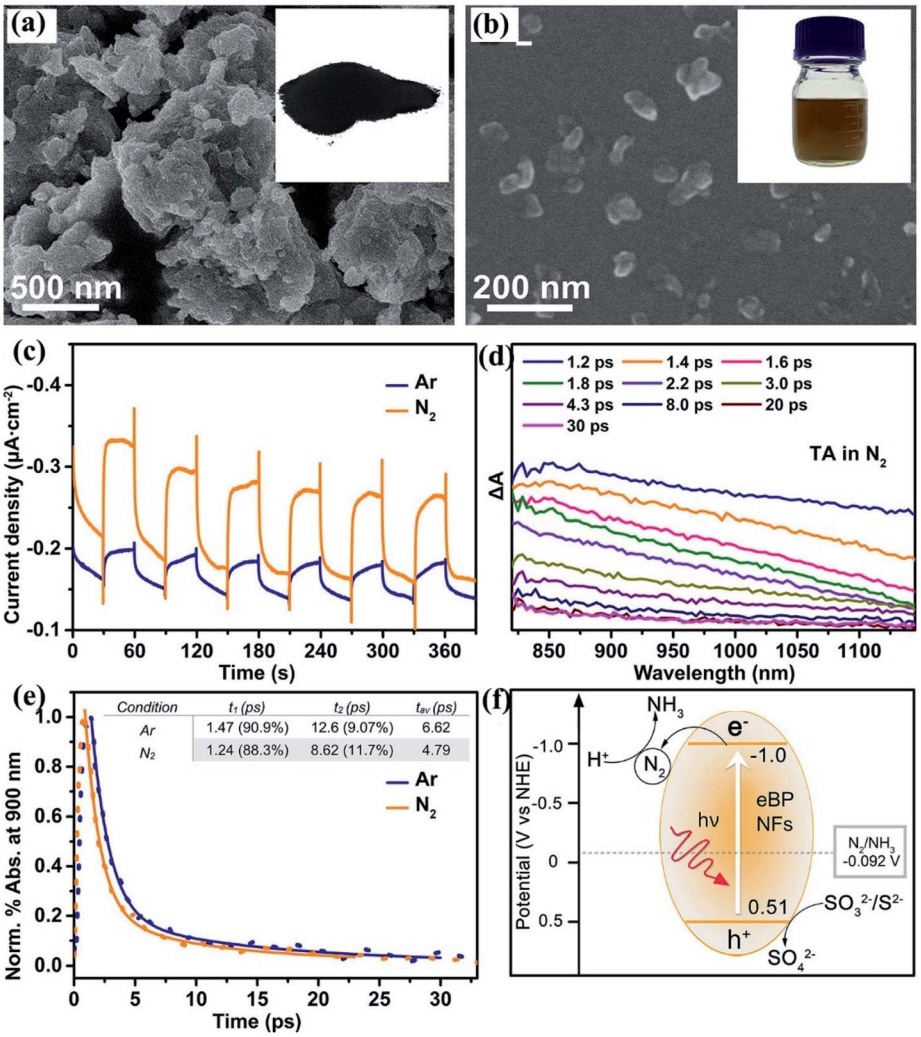

Fig. 6 (a) SEM image and inset photograph of the bulk BP powder; (b) SEM image of eBP NFs and inset photograph of the water suspension; (c) photocurrent response of BP in different atmospheres; (d) TA decay of eBP NFs in N_2 saturated water; (e) time profiles of normalized transient absorption at 900 nm; (f) schematic mechanism of semiconductor-based photocatalysis for nitrogen fixation.[21] Copyright 2020, American Chemical Society.

3.1.1 Oxygen vacancy. O vacancy is the most common active site in photocatalyst.[59] As a defect, it can capture electrons, adjust the energy band structure of catalyst,[60,61] enlarge the light response range,[33,62] improve the separation efficiency of photogenerated electrons and holes,[63–67] introduce more active sites to capture[52,68] and activate gas molecules.[69,70] A recent example, Fan *et al.* synthesized oxygen vacancy-induced $In(OH)_3$/carbon nitride (OV-$In(OH)_3$/CN)[71] and proved that $In(OH)_3$ in the heterojunction cannot generate photogenerated electrons under visible light, but its rich oxygen vacancies can receive and capture some excited electrons in g-C_3N_4, thereby improving the efficiency of charge separation and chemically adsorbing more nitrogen molecules. In addition, Wang and his coworkers reported a novel low-temperature method for the water-assisted self-assembly of Bi_5O_7Br nanotubes with an average diameter of 5 nm in 2017.[72] The prepared Bi_5O_7Br nanotubes photocatalyst has good nitrogen fixation performance, and the ammonia production rate reaches 1.38 mmol h^{-1} g^{-1}, which is attributed to the large amount of oxygen vacancy on the catalyst surface which is not easy to be oxidized. It was found that the photocatalyst will undergo the following four steps under the visible light irradiation(Fig. 7): (i) part of O_2 will escape from the surface of Bi_5O_7Br nanotubes to produce sufficient surface OVs; (ii) N_2 will be chemisorbed and activated on the O vacancy site; (iii) photoexcited electrons will transfer from the catalyst surface to activated N_2 and reduce it to NH_3; (iv) finally, after the catalytic reaction stops, the generated oxygen vacancy will capture the oxygen atoms in the water returns to its original state. Two years later, Di *et al.* found that surfactant polyvinylpyrrolidone (PVP) has a polyvinyl skeleton, which can interact strongly with the Bi^{3+}, O and N atoms of pyrrolidone ring, forming a passivation layer around the Bi_3O_4Br nucleus, and preventing the further growth of Bi_3O_4Br nanocrystals.[73] According to this characteristic, they have prepared Bi_3O_4Br nanocrystals with single cell thickness and rich oxygen vacancy. The Bi defect on the surface of Bi_3O_4Br

Table 1 Summary of nitrogen fixation performance of some photocatalysts containing vacancies

Types of vacancy		Samples	Light source	Hole scavenger	NH_4^+ generation rate	Atmosphere	Ref.
OVs		Bi_5OBr_7	Xe lamp	None	1.38 mmol h^{-1} g^{-1}	Air	72
		H_{200}-1.0Bi@BiOBr	300 W point light	None	181.2 μmol g^{-1} h^{-1}	N_2	53
		3% AgCl/&-Bi_2O_3	Xe lamp	None	606 μmol g^{-1} h^{-1}	N_2	61
		2% Co–$W_{18}O_{49}$	Xe lamp	Ethylene glycol	2752 μg g_{cat}^{-1}	Air	52
		Fe–$SrMoO_4$	Xe lamp	None	93.1 μM g^{-1} h^{-1}	N_2	60
		In_2O_3/In_2S_3	Xe lamp	None	40.04 μmol g^{-1} h^{-1}	N_2	62
		6% Cu–TiO_2	UV-vis	None	78.9 μmol g^{-1} h^{-1}	Air	63
		$TiO_2/ZnFe_2O_4$	Xe lamp	None	88.8 μmol g^{-1} L^{-1}	N_2	64
		WS_2TiO_2	AM 1.5G	None	1.39 mmol g^{-1} h^{-1}	N_2	50
		TiO_2	Xe lamp	Methanol	324.86 mmol h^{-1} g^{-1}	N_2	74
		OV-$In(OH)_3$/CN	Xe lamp	Triethanolamine	3.81 mM h^{-1} g^{-1}	N_2	71
NVs		Nv-CN	Sodium lamp	Methanol	5.5 mg L^{-1} h^{-1} g_{cat}^{-1}	50% O_2 + 50% N_2	86
		Nv&Sd–CN	Sodium lamp	None	6.2 mg L^{-1} h^{-1} g_{cat}^{-1}	N_2	88
		SiW_{12}/k-C_3N_4	Xe lamp	None	353.2 μM g^{-1} h^{-1}	Air	91
		Nv&Pd–CN	Sodium lamp	Methanol	7.5 mg L^{-1} h^{-1} g_{cat}^{-1}	N_2	89
		Nv&Od–CN	Xe lamp	Methanol	118.8 mg L^{-1} h^{-1} g_{cat}^{-1}	N_2	87
Other	C	g-C_3N_4-V	Xe lamp	None	32.4 mmol L−1 h−1	N_2	41
		I/g-C_3N_4	Xe lamp	Methanol	66.93 mg L−1 g_{cat}^{-1} h^{-1}	N_2	93
	S	CdS	Xe lamp	None	1.7 mg L^{-1} h^{-1}	Air	57
		SV-1T-MoS-CdS	AM 1.5G	Methanol	8220.83 μmol L^{-1} h^{-1} g^{-1}	N_2	19
	F	LaF_3:Yb^{3+}, Tm^{3+}/Pal	Xe lamp	1 mM Na_2SO_3	43.2 mg L^{-1}	Air	58
		Pr^{3+}:CeF_3	Xe lamp	Ethanol	629.16 ± 17.62 μmol L^{-1}	N_2	95

nanosheets could adjust the concentration of O vacancy, and the double vacancies act as the surface charge separation center, further promoting the charge separation of carriers, thus prolonging the life of carriers and increasing the photocatalytic nitrogen fixation activity to 30.9 times that of block Bi_3O_4Br.

However, too much O vacancy is not good, because oxygen vacancy can act as electron–hole recombination center, or destroy the original structure of nanocrystals, which will reduce the energy of light excited electrons.[35] Wang *et al.* compared the photocatalytic activity and oxygen vacancy concentration of TiO_2, TiO_2–H_2 and TiO_2–H_2–DA.[35] In this work, an ultra-thin amorphous layer was formed on TiO_2 surface in hydrogen atmosphere, which is rich in oxygen vacancy. However, with the increase of oxygen vacancy concentration, the ability of reducing nitrogen under visible light decreased. Therefore, after annealing TiO_2–H_2 with dicyandiamide (DA), part of the oxygen vacancies was remedied, and the catalytic activity of TiO_2–H_2–DA was increased to 1.2 mmol L^{-1} h^{-1}. A recent example, Zhang and his coworkers demonstrated that the excess of OVs in TiO_2 increased the adsorption and activation ability of N_2 molecules, but also showed disappointing activity due to the decrease of charge separation efficiency.[74] Excess OVs will become the recombination centers of photocarriers, which will greatly

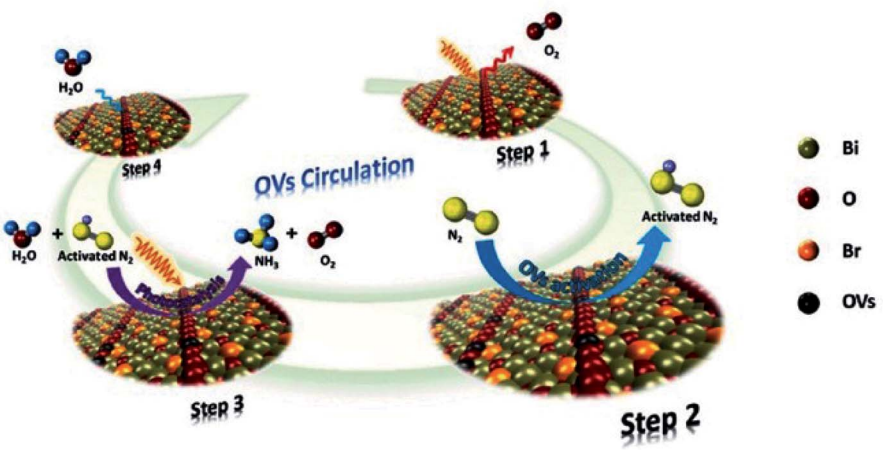

Fig. 7 Schematic illustration of the photocatalytic N_2 fixation model in which water serves as both the solvent and proton source, as well as the reversible creation of light-induced Ovs.[72] Copyright 2017, Wiley.

reduce the reduction ability of photogenerated electrons and have a negative impact on photocatalytic nitrogen fixation (Fig. 8). By using the reaction temperature (310–360 °C) and the reduction characteristics of $NaBH_4$, adjusting the oxygen vacancy concentration on TiO_2, the charge separation efficiency can be increased by three times under the condition of good chemisorption of N_2, which has an obvious activation effect on N_2. It was found that the optimum reaction temperature is 340 °C, and ammonia production is 324.86 mmol h^{-1} g^{-1}.

There are lots of researches on photocatalytic nitrogen fixation using oxygen vacancy as active site. In recent years, some researchers have proposed that the active sites of oxygen-enriched vacancy photocatalysts are metal ions exposed after oxygen is separated from the material, such as Ti^{3+} species,[48,75–77] Ce^{3+} species[40] and so on. However, most studies only pointed out oxygen vacancies as active sites, and did not describe specific active substances in detail. For example, Xie *et al.* reported the reliable exchange–correlation functionals, combined with the periodic slab model, to explore the specific mechanism of titanium oxide catalytic reduction of N_2 to NH_3 under the action of H_2O photolysis.[76] At the Ov site of the hydroxylated surface, the inert bond of the adsorbed N_2 is activated. At the same time, photogenerated electrons reduce the tetravalent Ti^{4+} species of the Ov site to trivalent Ti^{3+} species, and Ti^{3+} species as the active site promotes the photocatalytic nitrogen fixation. In addition, some researchers proposed that the oxygen vacancy of the catalyst itself interacts with the supported metal as the active center and active site of the catalytic reaction.[78–80] For instance, in the work of Sultana *et al.*, FeS_2–$FePCeO_2NSs$ ternary nanohybrid were synthesized by simple hydrothermal method and sulfonation phosphating technology.[78] They reported the Ov/Ce^{3+} and Fe–P act as active sites for N_2 molecule adsorption and activation.

3.1.2 Nitrogen vacancy. The number of catalysts with nitrogen vacancy as the active site is second only to that with oxygen vacancy as the active site, but generally, nitrogen vacancy only occurs in graphitic carbon nitride photocatalysts. As the active site, N vacancy can adsorb and activate N_2 molecule, and promote the transfer of photoelectron from catalyst to N_2 molecule.[81–83] Ren and his coworkers demonstrated that N

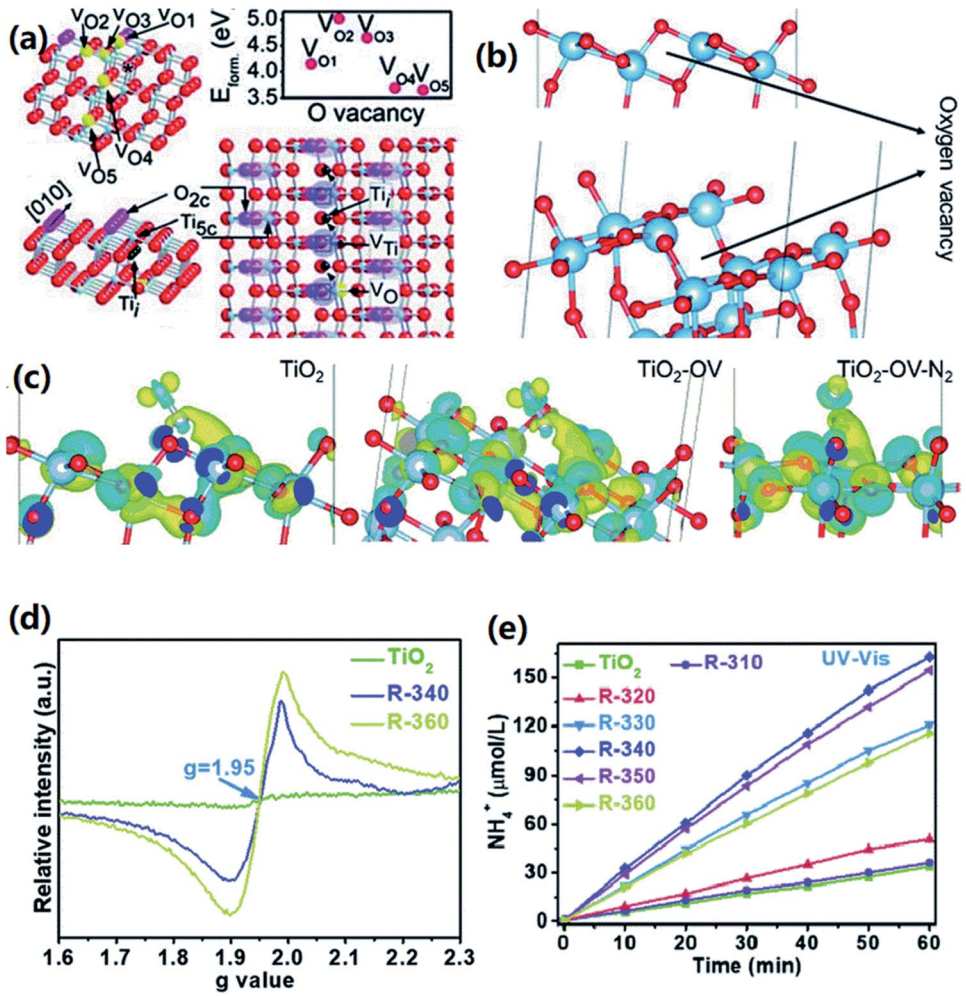

Fig. 8 (a and b) O-vacancy configuration of the (101)-crystal facet outer layer of anatase phase TiO_2; (c) Bader charge simulation and differential charge density data; (d) low temperature EPR spectra of anatase and reduced TiO_2; (e) the full-spectrum N_2 fixation data for anatase and reduced TiO_2.[74] Copyright 2020, Royal society of chemistry.

vacancy can not only improve the separation efficiency of photo induced carriers in g-C_3N_4, but also from the distortion conformation to activate more $n \rightarrow \pi^*$ transition of Nv-g-C_3N_4 and cause the red shift of optical absorption spectrum.[84]

There are many ways to increase the nitrogen vacancies of intrinsic photocatalyst, such as simple KOH etching, plasma treatment, *etc.* For example, Xue *et al.* modified g-C_3N_4 by alkali treatment. In the relevant peninsula, they used urea-assisted heat treatment to prepare porous g-C_3N_4 (NC-g-C_3N_4) with nitrogen defects and cyano groups.[43] Alkaline etching treatment can break the hydrogen bond of g-C_3N_4, accelerate the thermal polymerization of urea, and form nitrogen vacancies and cyano groups (Fig. 9). The presence of nitrogen vacancies expands the absorption of visible light by the catalyst, and at the same time, the cyano group helps to trap the photoelectrons generated by g-C_3N_4 under light and inhibits the recombination of carriers. In addition, more chemisorption sites (N vacancies) were generated to activate nitrogen molecules, which was beneficial to photocatalytic nitrogen fixation. The final activity of nitrogen fixation was 7.6 times than that of g-C_3N_4. In 2020, Wang and coworkers reported the method of modifying g-C_3N_4 with cyano and intercalated K^+.[85] It was proved that the cyano group in the catalyst could be regenerated under the action of intercalation K^+ (N vacancies increased), and the nitrogen fixation performance reached 3.42 mmol g^{-1} h^{-1}. The structure, specific surface area and morphology of catalyst will not be changed by plasma treatment, but nitrogen vacancies will be introduced into g-C_3N_4. For instance, Zhao *et al.* employed dielectric barrier discharge plasma treatment to prepared N vacancies embedded g-C_3N_4 (Nv-CN).[86] In the atmosphere of 50% N_2 and 50% O_2, the nitrogen fixation rate reaches 5.5 mg L^{-1} h^{-1} g_{cat}^{-1} under visible light.

For a g-C_3N_4 photocatalyst co-doped with non-metal atoms (such as P, S, O, B, *etc.*), the doped non-metallic elements can increase the activity of N vacancies and further improve the nitrogen-fixing performance. Recent research, hollow porous prismatic graphitic carbon nitride with nitrogen vacancies and oxygen doping was fabricated from dicyandiamidine with a facile two-step strategy of low-temperature hydrothermal method and calcination process.[87] In this work, the obtained catalyst (Nv&Od-CN) is hollow columnar and loose porous structure, which fully exposed the nitrogen vacancy as the active site with a yield of up to 118.8 mg L^{-1} h^{-1} g_{cat}^{-1}. Before that, nitrogen vacancy and sulfur co-doped g-C_3N_4,[88] nitrogen vacancy and phosphorus co-doped g-C_3N_4 were also reported.[25,89] Among them, the yield of N vacancy and S co-doped g-C_3N_4 (Nv&Sd-CN) produced by Li and his coworkers[88] using dicyandiamide and H_2S as raw materials by dielectric barrier discharge plasma treatment as high is as 6.2 mg L^{-1} h^{-1} g_{cat}^{-1}, which is 2.3 and 25.8 times higher than that of N doped g-C_3N_4 and g-C_3N_4, respectively. Shiraishi and coworkers made phosphor doped carbon nitride with nitrogen vacancy on the surface by a simple thermal condensation with hydroxyethyllidene diphosphonic acid (HEDP) and dicyandiamide as raw materials.[25] The doped P atom promoted the oxidation of water by valence band hole formed by light, while the N vacancy promoted the reduction of N_2 by conduction electron, and the ammonium ion production of catalyst under light was 4.9 μmol in 24 h. Wang *et al.*[89] used dicyandiamide and $(NH_4)_2HPO_4$ as raw materials to synthesize N vacancy and P-co-doped g-C_3N_4 (Nv&Pd-CN) by two-step calcination method. The yield of Co doped g-C_3N_4 is 7.5 mg L^{-1} h^{-1} g_{cat}^{-1}, which is 2.7 times and 28.8 times of that of single N vacancy-doped g-C_3N_4 and pure g-C_3N_4, respectively. In the latest example, Liang *et al.* made a catalyst with N vacancies and B doping.[90] They found that the B dopant could not only improve the adsorption and activation ability of N_2, but also maintain the high reduction ability of the catalyst.

Using the polyoxometalate (POM) is also one of the methods to increase the nitrogen fixation performance of g-C_3N_4 with N vacancy as the active site. For instance, Xiao *et al.* successfully covalently combined the polyoxometalate (POM) clusters of $[H_4SiO_{40}W_{12}]$ (SiW_{12}) with KOH modified graphitic carbon nitride nanosheets (k-C_3N_4) through phosphate bridging strategy.[91] k-C_3N_4 could not provide the protons needed for nitrogen fixation from water splitting, but POMs, as a cocatalyst, could enhance the ability of water oxidation and the adsorption and activation of N_2. As an effective adhesive and electron transfer chain, phosphoric acid anion can covalently combine POMs with k-C_3N_4 by replacing the surface hydroxyl group and

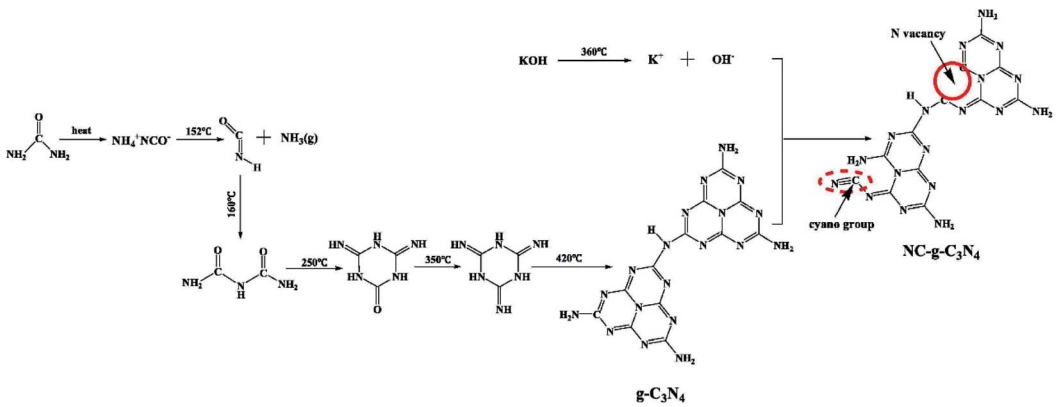

Fig. 9 Schematic diagram for the formation of NC-g-C_3N_4.[43] Copyright 2019, Elsevier.

enhance the interaction and transport of the support. The ammonia yield of the catalyst (Nv-CN/SiW_{12}) is 353.2 μM g^{-1} h^{-1}. In addition, Li and his coworkers compared four kinds of transition metal-substituted POMs and V-g-C_3N_4 composites as photocatalysts for nitrogen fixation.[92] The advantage of the catalyst is that the V-g-C_3N_4 nano sheet has a large specific surface area and rich N-defect sites, which is the main reason for the immobilization of POMs and the capture of N_2. In addition, the nano-sizes POMs could accept electrons and convert into reduced POMs under light conditions. As a strong photocatalyst, reduced POMs stimulated a lot of photo-generated electrons, which can be transferred rapidly to adsorbed N_2 on V-g-C_3N_4 nano sheet, weakening N≡N triple bond.

3.1.3 Other vacancies. In addition to oxygen and nitrogen vacancies, there are still some other vacancies, such as carbon vacancies, iodine vacancies, sulfur vacancies and fluorine vacancies in photocatalytic materials. The effect of these vacancies is analogous to that of O and N vacancies, which act as reaction sites to adsorb and activate nitrogen molecules and promote the effective separation of photogenerated carriers.

In addition to the N vacancy mentioned in the above section, there is also a C vacancy in the active site of the catalyst related to g-C_3N_4. For instance, Zhang *et al.* employed the high temperature peeling method to produce ultra-thin carbon nitride with loose structure and more carbon defects on the surface, which has a thin layer structure and more surface carbon vacancies, and can achieve effective charge separation.[41] In addition, the engineering carbon vacancies greatly promotes the adsorption and activation of nitrogen molecules, and greatly improves the nitrogen fixation activity of defective ultra-thin g-C_3N_4-V materials (Fig. 10). It was found that the pore volume of the catalyst increased after two times of thermal oxidation. The large increase of specific surface area shows that g-C_3N_4-V had a loose lamellar structure and was rich in mesopores. The existence of match pores is conducive to the adsorption of nitrogen molecules to participate in the activation reaction; more active sites will be exposed around the defects. After 100 minutes, the yield of ammonium ion reached 54 mmol L^{-1}. A recent example, the iodine-doped g-C_3N_4 with carbon vacancies was reported to be successful photocatalyst for nitrogen fixation in ambient condition.[93] Hu and his coworkers demonstrated that the band gap of iodine doped g-C_3N_4 with vacancy is smaller and the average PL lifetime is longer than that of pure g-C_3N_4. In other words, the photocatalyst response range is enlarged and the separation efficiency of photocarriers in iodized g-C_3N_4 is improved. Under visible light, the nitrogen fixation yield of photocatalyst is 66.93 mg L^{-1} g_{cat}^{-1} h^{-1}.

As the active site of adsorption and activation of nitrogen molecules, sulfur vacancy usually occurs in catalysts containing S elements such as CdS.[19] A rencent example, using thiourea, hexaammonium heptamolybdate tetrahydrate ($(NH_4)_6Mo_7O_{24}\cdot 4H_2O$), ethanol, methanol, ethylenediamine and cadmium chloride hemipentahydrate ($CdCl_2\cdot 2.5H_2O$) as raw materials, Sun and his coworkers successfully employed a simple one-step hydrothermal method to prepared the sulfur-rich oxygen doped 1T-MoS_2 nano sheet (SV-1T-MoS_2), and combined with CdS nano column to form a high-efficiency photocatalysis nitrogen fixing hybrid material (SV-1T-MoS_2-CdS).[19] In the catalyst, excessive thiourea adsorbed on the surface of the primary nano crystallite, which partially hindered the growth of the directional crystal and led to the formation of S vacancy. It was found that the conductivity of CdS is poor, which leads to slow electron transfer and long electron transfer time. However, the band gap width was reduced and negative displacement of CB occurs after adding the cocatalyst SV-1T-MoS_2, which was conducive to the transfer of electrons generated by photoexcitation from CB to VB. Surprisingly, under visible light, the yield of photocatalyst nitrogen fixation is as high as 8220.83 μmol L^{-1} h^{-1} g^{-1}. There are also many researches on CdS as photocatalyst. For example, Gao and his colleagues reported in 2019 that using NiS as cocatalyst reduced the overpotential of reducing N_2 and increased charge separation. Meanwhile, the S vacancy contained on the surface of CdS nanorods was used as the active site to adsorb and activate nitrogen molecules, and the final ammonium ion yield was 1.7 mg L^{-1} h^{-1}. In addition, He and his coworkers employed a selftemplated strategy to prepare In_2S_3 nanotubes in nitrogen

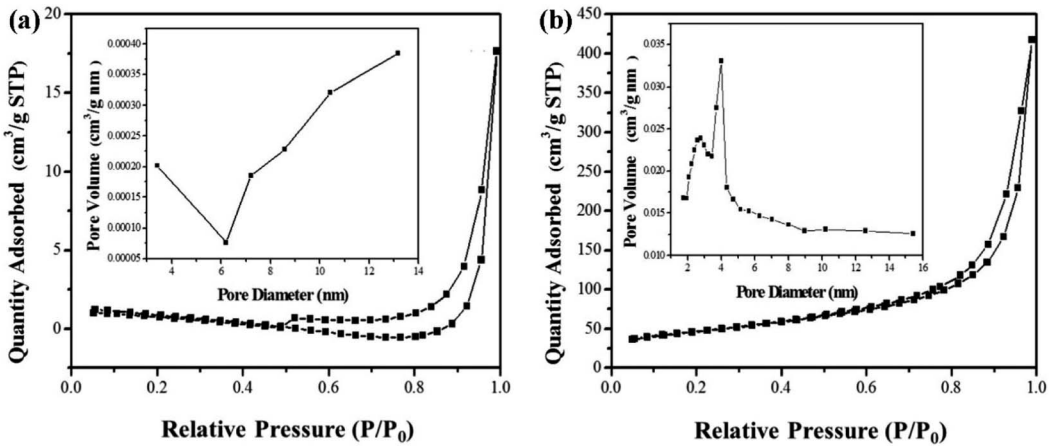

Fig. 10 Nitrogen absorption–desorption isotherm of (a) bulk g-C_3N_4 and (b) g-C_3N_4-V.[41] Copyright 2019, Elsevier.

atmosphere.[94] The S vacancy was produced when the material was calcined in nitrogen atmosphere (Fig. 11), which was made from indium nitrate ($In(NO_3)_3 \cdot xH_2O$), 1,4-benzenedicarboxylic acid (H_2BDC), thiourea, *N*,*N*-dimethylformamide (DMF), anhydrous ethanol and so on. As the active site of In_2S_3 catalyst in photocatalytic nitrogen fixation, S vacancy could effectively adsorb and activate nitrogen molecules. Meanwhile, the presence of sulfur vacancy enhances the absorption of light and promotes the separation and migration of photocarriers. Under visible light irradiation, the rate of reducing N_2 to NH_3 was 52.49 mmol h^{-1} g^{-1}, and the catalyst itself was stable.

Another common vacancy as the active site of photocatalytic nitrogen fixation is F vacancy. According to He and his coworkers, they have successfully prepared palygorskite (Pal) nanocomposites (LaF_3 : Yb^{3+}, Tm^{3+}/Pal) with sensitizer Yb^{3+} and activator Tm^{3+} co-doping LaF_3 by microwave hydrothermal method.[58] Due to the upconversion capability of this photocatalyst, it could be converted into visible light and ultraviolet light by near infrared, which improves the utilization of the whole solar spectrum. At the same time, LaF_3:Yb^{3+}, Tm^{3+} and modified Pal form an indirect Z-scheme heterostructure mediated by fluorine vacancy (FV), which is conducive to the separation of photogenerated electron–holes and the retention of high reduction oxidation potential. In addition, the F vacancy, as an active site, can effectively adsorb and activate nitrogen molecules. Under solar light irradiation, the total amount of ammonia can reach the highest of 43.2 mg L^{-1} under mild conditions. In 2019, Li and his coworkers successfully employed a microwave hydrothermal method to synthesized one dimensional attapulgite (ATP) mineral supported Pr^{3+} : CeF_3 nanocomposite.[95] It was found that the large amount of fluorine vacancies produced by the combination of some metal ions of ATP and crystal lattice of CeF_3 is the active site to promote the adsorption of N_2 and weaken the N≡N triple bond. The proper doping of Pr^{3+} can increase the utilization of solar energy, while the Z-scheme heterojunction constructed by PR^{3+}:CeF_3 and ATP can effectively improve the recombination of photogenerated electrons and holes, and retain high redox potential to reduce nitrogen molecules. Under the irradiation of solar energy, the nitrogen fixation rate of photocatalyst detected by Nessler's reagent is about 629.16 ± 17.62 μmol L^{-1}.

Therefore, based on the above discussion, this conclusion can be drawn: vacancy, as surface defect of photocatalyst, can effectively adsorb nitrogen in the atmosphere, activate nitrogen molecules and weaken N≡N triple bond of N_2 in the reaction of photocatalytic reduction of nitrogen. In some cases, vacancy could also adjust the energy band structure of catalyst, increase the utilization range of solar light, and transfer photoexcited electrons from catalyst to nitrogen molecules it adsorbs. The vacancy could be generated by various physical methods (such as calcination, plasma treatment, *etc.*) and chemical methods (such as chemical reaction with other compounds). At the same time, other atoms could be doped in the catalyst containing vacancy, so that the activation of vacancy to nitrogen is enhanced. As an active site, vacancy can adsorb nitrogen as well as other molecules. Taking oxygen vacancies on BiOBr as an example, it can adsorb both nitrogen and oxygen.[96] Although the oxygen generated *in situ* competes with nitrogen for surface adsorption, it can be removed from the reaction mixture in time under continuous N_2 purge, thereby avoiding further oxidation of NH_3 to NO_3^-. Oxygen vacancies can still provide a lot of nitrogen molecules for the photocatalytic nitrogen fixation of BiOBr. In addition, the concentration of vacancies is very important for the yield of photocatalytic nitrogen fixation. The more vacancies, the more active sites can participate in the reaction, the higher the nitrogen fixation effect. However, when there are too many vacancies, as discussed in Section 3.1.1, some vacancies may become the centers of charge recombination, which will inhibit the photocatalytic activity.

3.2 Metal doping site

Most of the metals acted as active sites in the photocatalyst of reducing nitrogen reaction are transition metals. Due of their high charge/radius ratio and space-d orbital for bonding, transition metals are easy to form stable coordination compounds with various ligands. In photocatalytic nitrogen fixation, the transition metal atoms (ions) in the catalyst can chemisorb nitrogen molecules and capture photoelectrons in time.

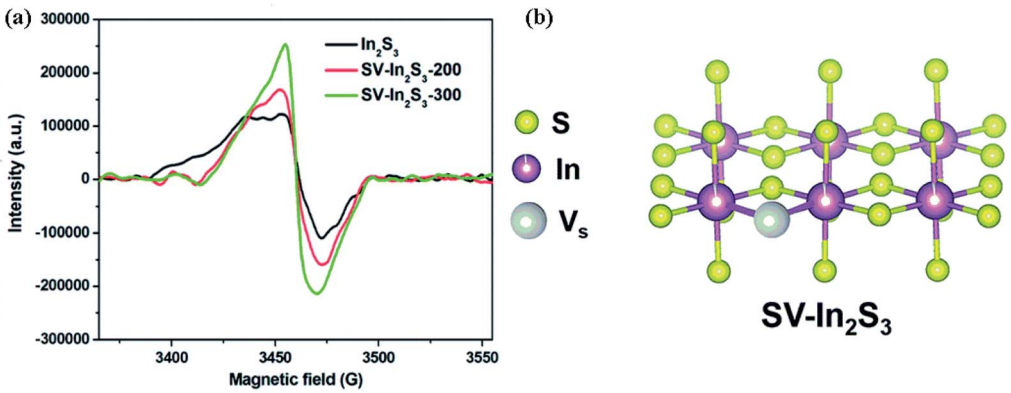

Fig. 11 (a) ESR spectra of In_2S_3, SV-In_2S_3-200 and SV-In_2S_3-300; (b) a schematic drawing of the crystal structures of SV-In_2S_3.[94] Copyright 2019, Royal Society of Chemistry.

Iron is the main active site in nitrogenase, thus Fe-containing[97] catalysts have been studied in photocatalytic nitrogen fixation, and Fe ions can act as active sites in photocatalytic nitrogen fixation. For instance, Yao and his coworkers compared the nitrogen reduction performance of the heterojunction photocatalyst constructed by g-C_3N_4 and Fe_2O_3 (g-C_3N_4/Fe_2O_3) with the composite photocatalyst of chelating Fe^{3+} ion and g-C_3N_4 nano sheet (CNNs) by EDTA (Fe-EDTA-CNNs).[98] They think that N_2 has lone pair electrons, and the empty d orbital of Fe atom can accept lone pair electrons. In addition, Fe atom has independent d electrons, which can be supplied to the antibinding orbital to strengthen N–Fe bond and weaken N≡N triple bond. It was found that the Fe active sites are highly dispersed and stable in 2D CNNs due to the complexation of EDTA. Under the irradiation of visible light, Fe-EDTA-CNNs photocatalyst generates photogenerated electrons and holes. Under the electric traction effect of Fe-EDTA group, photoexcited electrons accumulate on Fe-EDTA, which are transferred to adsorbed N_2 by Fe^{3+}, and finally combine with protons in water to form ammonium ions (Fig. 12). Impressively, compared with other reported g-C_3N_4 catalysts, Fe-EDTA-CNNs photocatalyst showed a much higher activity for N_2 fixation (49.252 mmol L^{-1} h^{-1}).

Transition metal Ru exhibits a lower N_2 reduction overpotential than Fe. Therefore, in the experiment of studying photocatalytic nitrogen fixation, Ru-containing photocatalyst is the choice of some researchers. Liu and his coworkers demonstrated that the monoatomic metal dispersed on the support showed the homogeneity of catalytic active sites, the maximum efficiency of metal utilization and the low coordination environment of metal atoms.[99] The Ru–TiO_2 Ns catalyst was obtained by mixing the ultrasonic dispersed TiO_2 in ethanol with ruthenium chloride ethanol solution. Under the irradiation of sunlight, the photocatalyst loaded with 1 wt% of Ru reduced N_2 to ammonia at the highest rate of 56.3 μg h^{-1} $g_{cat}{}^{-1}$. After a series of analysis, they thought that Ru atoms deposited on the O vacancy of TiO_2 surface is the center of nitrogen molecules adsorption and activation, and could improve the separation of charge carriers, thus promoting the performance of photocatalysis. According to reports by Awati and his coworkers, they used organic solvent extraction to extract the fine graphite-like carbon layer in coal, and obtained metals containing Ca^{2+}, Ti^{4+}, Ti^{3+},[100] Fe^{2+}, Al^{3+}, Si^{4+}, C, N, O, *etc.* The coal-based carbon nanosheets (CNs), and finally ruthenium (Ru) nanoparticles were loaded *in situ* from $RuCl_3 \cdot 3H_2O$ onto the prepared catalyst to prepare a Ru/CNs composite catalyst.[101] In this work, metal Ru provides more active sites for CNS, promotes the adsorption and activation of nitrogen molecules on the catalyst, and increases the ammonia yield to 55.325 μmol L^{-1} h^{-1}. A recent example, using Ti_3AlC_2 as the precursor, Hao and coworkers synthesized MXene by HF etching, and completed the growth of RuO_2 nanoparticles and TiO_2 on the substrate MXene by hydrothermal reaction.[102] It was found that the ultrafine RuO_2 nanoparticles with a large number of metal Ru(0) centers can effectively reduce the reduction barrier and increase the ammonia yield as the active site of reducing nitrogen. Although most studies have shown that metal atoms are evenly loaded on the layered material structure, and better play its role as an active site, there are exceptions in everything. Liu and his coworkers reported an interesting discovery, they demonstrated that even dispersion of atoms on the support surface is not necessarily the best way to improve the efficiency of photocatalytic nitrogen fixation.[103] They compared the catalytic performance of bulk carbon nitride (B-g-C_3N_4) and exfoliated carbon nitride (E-g-C_3N_4) catalysts supported with K and Ru. After a series of analysis, they concluded that although Ru–K/E-g-C_3N_4 has larger specific surface area and more effective electron hole separation than Ru–K/B-g-C_3N_4, and Ru is evenly dispersed on the surface of E-g-C_3N_4, the catalytic nitrogen fixation activity of Ru–K/B-g-C_3N_4 is better than that of Ru–K/E-g-C_3N_4. The reason is that Ru is distributed on the edge steps of Ru–K/B-g-C_3N_4. Due to the strong combination between Ru cluster and support, the interaction between N_2 and Ru cluster is reduced. The energy barrier of Ru–K/B-g-C_3N_4 is low. In the photocatalytic synthesis of ammonia, Ru cluster can not only enhance the charge generated by light adsorption, but also provide an active center for proton reduction and ammonia synthesis. Therefore, Ru–K/B-g-C_3N_4 has stronger photocatalytic nitrogen fixation ability.

In addition to the above mentioned Fe,[104] Ru metals as active sites, Mo,[105] Co,[20,106,107] Li,[108] Ag,[109] Ce[110] and Te[84] are also common as active centers for photocatalytic nitrogen fixation. For instance, a novel ternary MoS_2/C–ZnO composite synthesized by Xing and his colleagues through hydrothermal method and photodeposition method. In the photocatalytic reduction of nitrogen, Mo acts as the active site, receives photoelectrons transmitted from the carbon layer, and transfers electrons to the adsorbed nitrogen fraction.[111] Guo and coworkers prepared polyatomic Mo doped carbon nitride with urea and $Na_2MoO_4 \cdot 2H_2O$ as raw materials.[112] The isolated Mo centers were fixed by coordination with two N donors on the *in situ* formed polymeric carbonitride, forming two coordinated MoN_2 species. As an active site, the low coordination Mo center strongly adsorbs nitrogen molecules through end-on configuration, which shortens the bond length and weakens the bond energy of N≡N bond. When ethanol is used as a hole cleaner, the ammonia yield under visible light is as high as 830 μmol $g_{cat}{}^{-1}$ h^{-1}. Wang and his coworkers prepared three-dimensional cobalt doped

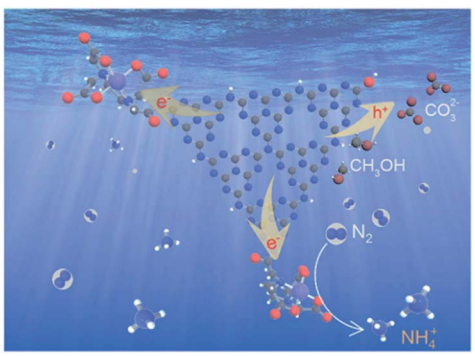

Fig. 12 Possible mechanism for photocatalytic nitrogen fixation of Fe-EDTA-CNNS.[98] Copyright 2019, Royal Society of Chemistry.

graphite carbon nitride by molten salt assistant method.[106] On this catalyst, cobalt exists in the form of Co–N coordination bond (Fig. 13). As an active site, it can chemically adsorb and activate N_2 molecule, and promote the electron transfer from catalyst to nitrogen molecules. In this work, they carried out density functional theory (DFT) simulation, and found that cobalt doping can not only prolong the activation of N≡N bond on N_2 molecule, but also capture photoelectrons and improve the efficiency of electron hole separation of g-C_3N_4. The d orbital of cobalt can be used as a channel for transition metal to transfer electrons to N_2 molecule, which improves the optical fixation ability of N_2 molecule. Under visible light irradiation, the NH_4^+ yield of Co doped g-C_3N_4 is 5.8 mg L^{-1} h^{-1} g_{cat}^{-1}, 24 times higher than that of bulk g-C_3N_4. In the same study, Li doped g-C_3N_4 catalyst made by Gu *et al.* was used for photocatalytic nitrogen fixation.[108] It was found that Li existed in the form of Li–N bond. As an active site in photocatalytic nitrogen fixation, Li chemically adsorbed and activated nitrogen molecules, and transferred photoelectrons from the catalyst to nitrogen gas. Ag, as a kind of precious metal, could improve the activity of the catalyst after plasma treatment. Xing and his coworkers synthesized Ag/$KNbO_3$ photocatalyst by photodeposition and hydrothermal deposition.[113] Ag nanoparticles (Ag NPs) could capture electrons from the surface of photocatalyst and increase the separation of photogenerated carriers. At the same time, due to the surface plasmon resonance effect of silver nanoparticles, it could promote the absorption of visible light. With the help of Ag NPs as the active site, the ammonia yield of photocatalyst Ag/$KNbO_3$ containing 0.5% Ag is 385.0 μmol L^{-1} g^{-1} h^{-1}, which is 4 times of that of KNbO.

To sum up, in the photocatalytic nitrogen fixation, the active sites on the catalyst play the role of adsorbing and activating nitrogen molecules, transferring photoelectrons from the catalyst to the adsorbed nitrogen molecules. Some of them are the vacancies generated by the catalyst itself through various treatments as active sites, and some of them are the foreign elements doped through various measures as the active site. While these vacancies or metal elements adsorb and activate nitrogen molecules, they can sometimes adjust the band gap of the catalyst and increase the light absorption range. It is immensely helpful to fully understand the active site of photocatalyst in nitrogen fixation reaction for improving the activity of photocatalyst in nitrogen fixation. However, at present, many studies have not really indicated the active site in the catalyst, and the detection of the active site has not been unified. That because the determination of the active site is basically directly based on DFT calculation and some researchers indirectly prove

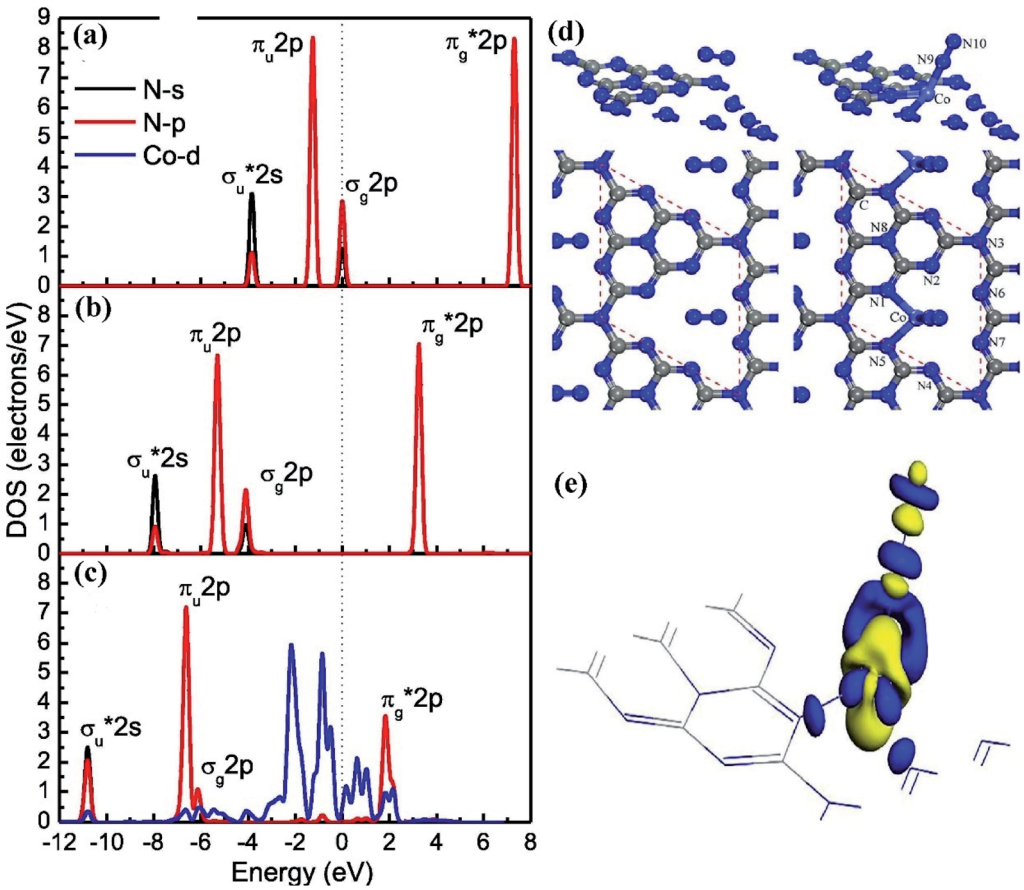

Fig. 13 Density of states of (a) free N_2, (b) N_2 adsorbed on bulk g-C_3N_4 and (c) N_2 adsorbed on Co-GCN(1); (d) the charge density difference of the N_2 molecule adsorbed on Co-GCN(1); (e) the optimal N_2 adsorption models on bulk g-C_3N_4 (left) and Co-GCN(1) (right).[106] Copyright 2019, Elsevier.

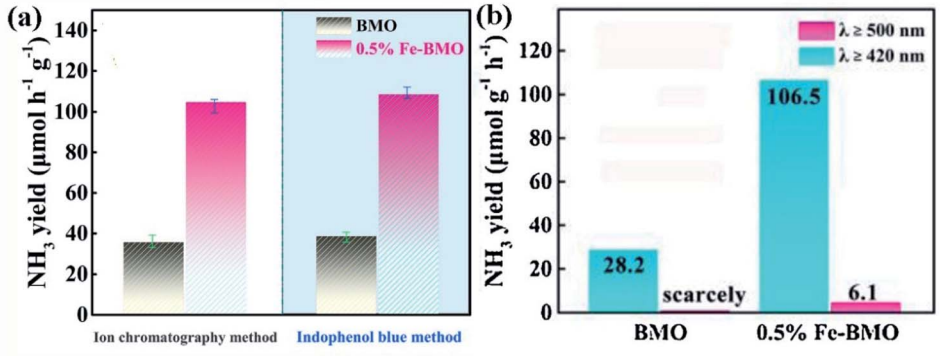

Fig. 14 Photocatalytic nitrogen fixation of BMO and 0.5% Fe-BMO with (a) indophenol blue method and ion chromatography method, (b) Nesslers reagent.[118] Copyright 2019, Elsevier.

the existence of the active site using N_2 absorption–desorption isotherm, the temperature programmed desorption of N_2 (N_2-TPD) and *in situ* FTIR spectroscopy. It's still needs to develop more intuitive and simple methods to determine the active site of nitrogen. There is still a long way to go in the research of photocatalyst in nitrogen fixation.

4. Method for determination of ammonia content

The accurate determination of ammonia yield is especially important to explain the nitrogen fixation performance of photocatalyst. At present, almost all the researches on photocatalytic reduction of nitrogen use the following three methods to test the amount of ammonia: ion chromatography,[48] Nessler's reagent[114] and indophenol blue method.[115] Moreover, a more advanced method for quantitative ammonia measurement has now been discovered firstly, which is gas chromatographic method for *in situ* ammonia quantification.[116] Here is a brief analysis of three common methods, namely the indophenol blue method, Nessler's reagent method and ion chromatography. Among them, Nessler's reagent and indophenol blue method can be attributed to spectrophotometry. Compared with the other too methods, ion chromatography has

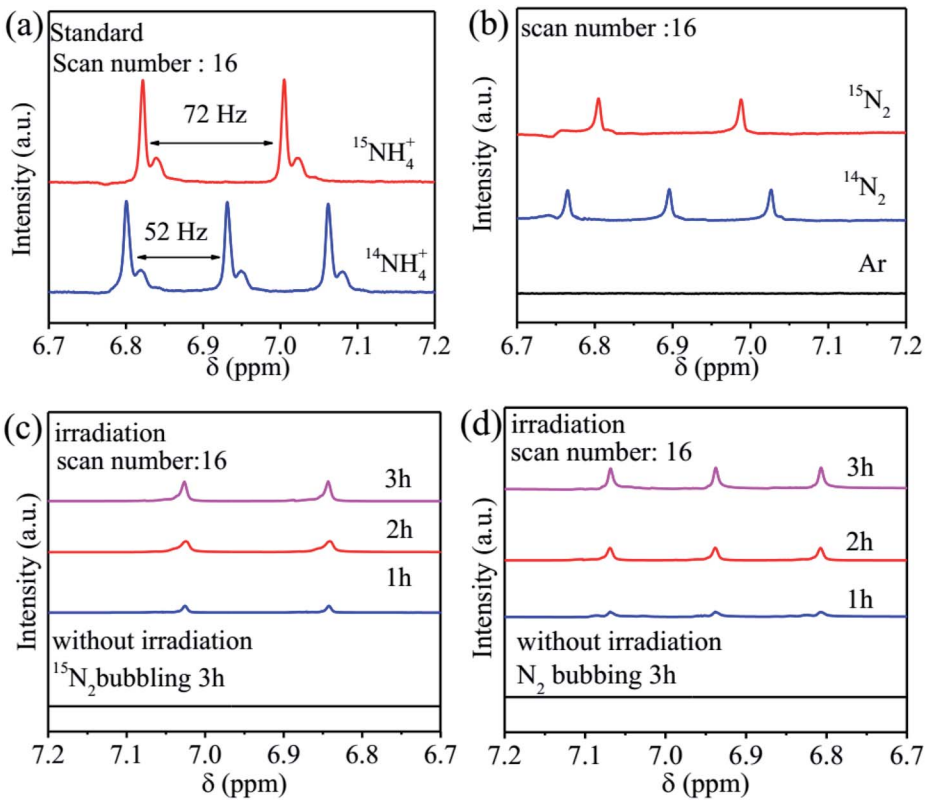

Fig. 15 (a) ^{1}H nuclear magnetic resonance (NMR) spectra were calibrated using dimethyl sulphoxide (DMSO) as an internal standard; (b) the chemical shifts in the spectra were obtained for the 10 vol% methanol solution with $^{15}N_2$, $^{14}N_2$, or Ar as the feeding gas, respectively; the chemical shifts in the spectra were obtained for the vol% methanol solution with $^{15}N_2$ (c) and $^{14}N_2$ (d) as the feeding gas.[20] Copyright 2019, Wiley.

higher efficiency (multiple components and cations can be detected at the same time in a short time), higher sensitivity (the concentration can be from several to hundreds of mg L^{-1}), high selectivity (the inorganic cations and organic cations can be quantified), better stability and compatibility (the pH stability of ion chromatography column packing is higher and the application scope is wider),[117] but its price is expensive and there will be large errors in the measurement of ammonia when there is sacrificial agent. The Nessler's reagent method and indophenol blue method are used more economically, but the ammonia content measured with indophenol is very inaccurate when the acid condition and ammonia concentration are higher than 500 g L^{-1}.[117]

Therefore, when measuring the rate of reducing nitrogen by photocatalyst under light irradiation, we need to consider all kinds of situations: whether there is sacrificial agent, pH value, approximate concentration of ammonia and economic conditions. In one work, it is sometimes considered to use a variety of ammonia measurement methods to ensure the accuracy of experimental data. So far, some studies have used indophenol blue method and ion chromatography,[102] some have used indophenol blue method and Nessler's reagent method at the same time,[60] some have even used three methods to explore nitrogen fixation efficiency.[69] For example, Meng and his coworkers tested the ammonia production of the Fe-doped Bi_2MoO_6 photocatalyst in the solution after reaction under light with Nessler's reagent, indophenol blue method and ion spectrum method, and finally confirmed that the data obtained by the three methods were almost the same(Fig. 14).[118]

The biggest advantage of gas chromatographic method is that it can detect the real-time concentration of ammonia in the reaction process online. In addition, the sample processing and preparation time is greatly reduced, which reduces the working time of the experimenter.[116] Unfortunately, there are not many applications of this method at present, and there are too few related documents. But because of its unique advantages, it is expected to have more applications in the future.

In addition, the synthesis of many photocatalysts involves the use of nitrogen-containing compounds. Some photocatalysts are also rich in nitrogen. In the process of photocatalytic reaction, some nitrogen may be lost to the reaction medium, which makes the quantitative complexity of ammonia. Therefore, isotope labeling is widely used to detect the rate of photocatalytic nitrogen fixation. For example, in the study of Yuan *et al.*, For the prepared graphite carbon nitride nanosheets (Ru-vs-cos/CN) photocatalysts, they used ^1H nuclear magnetic resonance (^1H NMR) spectroscopy to further confirm that only $^{14}N_2$ or $^{15}N_2$ can be used as a nitrogen source to feed gas NH_3 is produced. The signal intensity of $^{15}NH_4^+$ or $^{14}NH_4^+$ produced is positively correlated with the reaction time under irradiation (Fig. 15), which made the quantification of ammonia simple and clear.[20]

5. Conclusions and outlook

It has been a hundred years since the discovery and use of the Haber–Bosch process. Scientists have been exploring new, milder methods nitrogen fixation reactions. Photocatalytic nitrogen fixation can use sunlight to reduce nitrogen molecules in the air under mild conditions. In recent years, with the efforts of generations of researchers, photocatalytic nitrogen fixation technology has achieved good results, but it is still far from being used in industrial production. In the photocatalytic nitrogen reduction reaction, the photocatalyst must simultaneously meet three conditions: high utilization rate of light, high separation rate of photogenerated electron–holes, and high adsorption and activation ability of nitrogen molecules. Increasing material surface defects, loading precious metal atoms, doping various atoms or ions, constructing heterojunctions, and supporting auxiliary catalysts, *etc.* are all effective methods to improve the above three conditions. These methods, in the final analysis, have a common effect, which increases the active sites on the photocatalyst surface. The active site plays an important role in adsorbing and activating N_2 molecules and transferring photogenerated electrons to the adsorbed nitrogen molecules in the photocatalytic nitrogen fixation reaction. Common active sites are various vacancies and metal dopants. O vacancies are the most common active sites. In many photocatalysts that use O vacancies as active sites, the presence of O vacancies also enhances the light absorption range of the catalyst, but the concentration of O vacancies cannot be too much. Excessive O vacancies will become the electron–hole recombination center, thereby inhibiting the reduction of nitrogen. In g-C_3N_4-based photocatalysts, N vacancies is developed as active sites. Increasing the number of N vacancies is one of the ways to improve the ability of catalytic nitrogen fixation. To achieve non-metal (P, S, O, *etc.*) and N vacancies Co-doping is also an effective method to enhance the activity of nitrogen fixation. Doped nonmetals can effectively enhance the activity of N vacancies. In recent years, photocatalytic nitrogen fixation catalysts with metal doped bodies as active sites have become very popular. The transition metal Ru, Fe, Mo, Co, *etc.*, the coordinated unsaturated bond of the rare earth element Ce, the Li–N bond formed by metal Li, *etc.* The electronic feedback can weaken the N≡N triple bond, activate the N_2 molecule, and promote the reduction of N_2 to NH_3.

Besides aforementioned achievements, to improve the reducing ability of the photocatalyst for nitrogen under sunlight, much attention needs to be paid to improving the number and performance of active sites on the surface of the catalyst. Thus, many aspects need to be studied and explored. First, in the subsequent nitrogen fixation studies, it may be possible to consider combining multiple active sites for nitrogen fixation testing, such as the exploration of nitrogen fixation in the presence of nitrogen vacancies and oxygen vacancies, oxygen vacancies and metal sites or metal and metal sites. Secondly, nitrogen has low solubility in water. Thus, regarding the existing aqueous photocatalytic nitrogen fixation reaction system, some improvements could be considered, such as the ratio of catalyst to water, the use of ionic liquids, developing the gas–solid system and the use of heat for light conversion instead of cooling water only. In addition, in future research, the calculation of the active site and the *in situ* test

may be used to calculate the catalytic reaction process, and a suitable catalyst could be designed according to the calculation results.

Disclaimer

The author cannot accept liability for any errors in the experimental data referenced in this article.

Conflicts of interest

There are no conflicts to declare.

Acknowledgements

This work was sponsored by National Natural Science Foundation of China (Grant No. 21802078 and 21965027) and Natural Science Foundation of Ningxia, China (2018AAC03053).

References

1 C. X. Guo, J. R. Ran, A. Vasileff and S. Z. Qiao, *Energy Environ. Sci.*, 2018, **11**, 45–56.
2 M. H. Vu, M. Sakar, S. A. Hassanzadeh-Tabrizi and T. O. Do, *Adv. Mater. Interfaces*, 2019, **6**, 1900091.
3 H. Mou, J. Wang, D. Yu, D. Zhang, W. Chen, Y. Wang, D. Wang and T. Mu, *ACS Appl. Mater. Interfaces*, 2019, **11**, 44360–44365.
4 L. Ye, C. Han, Z. Ma, Y. Leng, J. Li, X. Ji, D. Bi, H. Xie and Z. Huang, *Chem. Eng. J.*, 2017, **307**, 311–318.
5 Y. Ren, D. Zeng and W.-J. Ong, *Chin. J. Catal.*, 2019, **40**, 289–319.
6 Y. Liao, J. Lin, B. Cui, G. Xie and S. Hu, *J. Photochem. Photobiol., A*, 2020, **387**, 112100.
7 S. Cao, H. Chen, F. Jiang and X. Wang, *Appl. Catal., B*, 2018, **224**, 222–229.
8 B. M. Comer and A. J. Medford, *ACS Sustainable Chem. Eng.*, 2018, **6**, 4648–4660.
9 X. Rong, Y. Mao, J. Xu, X. Zhang, L. Zhang, X. Zhou, F. Qiu and Z. Wu, *Catal. Commun.*, 2018, **116**, 16–19.
10 C. Tian, W. Sheng, H. Tan, H. Jiang and C. Xiong, *ACS Appl. Mater. Interfaces*, 2018, **10**, 37453–37460.
11 H. Mou, J. Wang, D. Zhang, D. Yu, W. Chen, D. Wang and T. Mu, *J. Mater. Chem. A*, 2019, **7**, 5719–5725.
12 C. Mao, J. Wang, Y. Zou, H. Li, G. Zhan, J. Li, J. Zhao and L. Zhang, *Green Chem.*, 2019, **21**, 2852–2867.
13 H. Diarmand-Khalilabad, A. Habibi-Yangjeh, D. Seifzadeh, S. Asadzadeh-Khaneghah and E. Vesali-Kermani, *Ceram. Int.*, 2019, **45**, 2542–2555.
14 S. Liu, S. Wang, Y. Jiang, Z. Zhao, G. Jiang and Z. Sun, *Chem. Eng. J.*, 2019, **373**, 572–579.
15 X. Gao, Y. Shang, L. Liu and K. Gao, *J. Alloys Compd.*, 2019, **803**, 565–575.
16 C. Guo, J. Ran, A. Vasileff and S.-Z. Qiao, *Energy Environ. Sci.*, 2018, **11**, 45–56.
17 M. Cheng, C. Xiao and Y. Xie, *J. Mater. Chem. A*, 2019, **7**, 19616–19633.
18 J. Qin, X. Hu, X. Li, Z. Yin, B. Liu and K.-h. Lam, *Nano Energy*, 2019, **61**, 27–35.
19 B. Sun, Z. Liang, Y. Qian, X. Xu, Y. Han and J. Tian, *ACS Appl. Mater. Interfaces*, 2020, **12**, 7257–7269.
20 J. Yuan, X. Yi, Y. Tang, M. Liu and C. Liu, *Adv. Funct. Mater.*, 2019, **30**, 1906983.
21 S. Bian, M. Wen, J. Wang, N. Yang, P. K. Chu and X.-F. Yu, *J. Phys. Chem. Lett.*, 2020, **11**, 1052–1058.
22 X. Niu, Q. Zhu, S. Jiang and Q. Zhang, *J. Phys. Chem. Lett.*, 2020, **11**, 9579–9586.
23 S. Zhang, Y. Zhao, R. Shi, C. Zhou, G. I. N. Waterhouse, L.-Z. Wu, C.-H. Tung and T. Zhang, *Adv. Energy Mater.*, 2020, **10**, 1901973.
24 Y. Zhao, L. Zheng, R. Shi, S. Zhang, X. Bian, F. Wu, X. Cao, G. I. N. Waterhouse and T. Zhang, *Adv. Energy Mater.*, 2020, **10**, 2002199.
25 Y. Shiraishi, S. Shiota, Y. Kofuji, M. Hashimoto, K. Chishiro, H. Hirakawa, S. Tanaka, S. Ichikawa and T. Hirai, *ACS Appl. Energy Mater.*, 2018, **1**, 4169–4177.
26 X. Cui, C. Tang and Q. Zhang, *Adv. Energy Mater.*, 2018, **8**, 1800369.
27 A. Shi, H. Li, S. Yin, Z. Hou, J. Rong, J. Zhang and Y. Wang, *Appl. Catal., B*, 2018, **235**, 197–206.
28 X.-M. Gao, Y.-Y. Shang, L.-B. Liu and W. Nie, *J. Inorg. Mater.*, 2019, **34**, 967–973.
29 H. Maimaitizi, A. Abulizi, T. Zhang, K. Okitsu and J.-J. Zhu, *Ultrason. Sonochem.*, 2020, **63**, 104956.
30 D. Wu, R. Wang, C. Yang, Y. An, H. Lu, H. Wang, K. Cao, Z. Gao, W. Zhang, F. Xu and K. Jiang, *J. Colloid Interface Sci.*, 2019, **556**, 111–119.
31 Y. J. Xue, X. K. Kong, Y. C. Guo, Z. Q. Liang, H. Z. Cui and J. Tian, *J. Materiomics*, 2020, **6**, 128–137.
32 Y. Chen, C. Zhao, S. Ma, P. Xing, X. Hu, Y. Wu and Y. He, *Inorg. Chem. Front.*, 2019, **6**, 3083–3092.
33 X. Yan, D. Dai, K. Ma, S. Zuo, W. Liu, X. Li and C. Yao, *Front. Mater. Sci.*, 2019, **14**, 43–51.
34 N. I. E. Wei, L. I. U. Li-Bo, S. Yan-Yan and G. A. O. Xiao-Ming, *J. Inorg. Mater.*, 2019, **34**, 967–973.
35 J. Wang, W. Lin, Y. Ran, J. Cui, L. Wang, X. Yu and Y. Zhang, *J. Phys. Chem. C*, 2020, **124**, 1253–1259.
36 P. Qiu, C. Xu, N. Zhou, H. Chen and F. Jiang, *Appl. Catal., B*, 2018, **221**, 27–35.
37 T. Fei, L. Yu, Z. Liu, Y. Song, F. Xu, Z. Mo, C. Liu, J. Deng, H. Ji, M. Cheng, Y. Lei, H. Xu and H. Li, *J. Colloid Interface Sci.*, 2019, **557**, 498–505.
38 W. Chen, X.-H. Li, P. He, T. Wang, X.-W. Zhang and Y.-G. Li, *ChemSusChem*, 2020, **13**, 2769–2778.
39 H. Wang, R. Zhao, J. Qin, H. Hu, X. Fan, X. Cao and D. Wang, *ACS Appl. Mater. Interfaces*, 2019, **11**, 44249–44262.
40 X. Feng, H. Chen, F. Jiang and X. Wang, *Catal. Sci. Technol.*, 2019, **9**, 2849–2857.
41 Y. Zhang, J. Di, P. Ding, J. Zhao, K. Gu, X. Chen, C. Yan, S. Yin, J. Xia and H. Li, *J. Colloid Interface Sci.*, 2019, **553**, 530–539.
42 W. Gao, X. Li, S. Luo, Z. Luo, X. Zhang, R. Huang and M. Luo, *J. Colloid Interface Sci.*, 2020, **585**, 20–29.

43 Y. Xue, Y. Guo, Z. Liang, H. Cui and J. Tian, *J. Colloid Interface Sci.*, 2019, **556**, 206–213.
44 J. Li, H. Li, G. Zhan and L. Zhang, *Acc. Chem. Res.*, 2017, **50**, 112–121.
45 S. H. Wang, W. Wei, X. S. Lv, B. B. Huang and Y. Dai, *J. Mater. Chem. A*, 2020, **8**, 1378–1385.
46 C. Xiao, H. Wang, L. Zhang, S. Sun and W. Wang, *Chemcatchem*, 2019, **11**, 6467–6472.
47 S.-X. Wang, H. Maimaiti, B. Xu, Y. Guo, P.-s. Zhai and H.-z. Zhang, *J. Phys. Chem. C*, 2019, **123**, 31119–31129.
48 H. Hirakawa, M. Hashimoto, Y. Shiraishi and T. Hirai, *J. Am. Chem. Soc.*, 2017, **139**, 10929–10936.
49 H.-P. Jia and E. A. Quadrelli, *Chem. Soc. Rev.*, 2014, **43**, 547–564.
50 L. Shi, Z. Li, L. Ju, A. Carrasco-Pena, N. Orlovskaya, H. Zhou and Y. Yang, *J. Mater. Chem. A*, 2020, **8**, 1059–1065.
51 Q. Wang, W. Wang, L. Zhong, D. Liu, X. Cao and F. Cui, *Appl. Catal., B*, 2018, **220**, 290–302.
52 J. Ge, J. Xu, Y. Liu, L. Zhang, L. Wang and D. Wu, *Nano*, 2019, **14**, 1950143.
53 C. Hua, X. Dong, Y. Wang, N. Zheng, H. Ma and X. Zhang, *J. Mater. Sci.*, 2019, **54**, 9397–9413.
54 Y. Shiraishi, K. Chishiro, S. Tanaka and T. Hirai, *Langmuir*, 2020, **36**, 734–741.
55 D. Vidyasagar, A. Balapure, S. G. Ghugal, A. G. Shende and S. S. Umare, *Phys. Status Solidi A*, 2019, **216**, 1900212.
56 R. Ding, S. Cao, H. Chen, F. Jiang and X. Wang, *Colloids Surf., A*, 2019, **563**, 263–270.
57 X. Gao, L. An, D. Qu, W. Jiang, Y. Chai, S. Sun, X. Liu and Z. Sun, *Sci. Bull.*, 2019, **64**, 918–925.
58 C. He, X. Li, X. Chen, S. Ma, X. Yan, Y. Zhang, S. Zuo and C. Yao, *Appl. Clay Sci.*, 2020, **184**, 105398.
59 P. Li, Z. Zhou, Q. Wang, M. Guo, S. Chen, J. Low, R. Long, W. Liu, P. Ding, Y. Wu and Y. Xiong, *J. Am. Chem. Soc.*, 2020, **142**, 12430–12439.
60 J. Luo, X. Bai, Q. Li, X. Yu, C. Li, Z. Wang, W. Wu, Y. Liang, Z. Zhao and H. Liu, *Nano Energy*, 2019, **66**, 104187.
61 X. Gao, Y. Shang, L. Liu and F. Fu, *J. Catal.*, 2019, **371**, 71–80.
62 H. Xu, Y. Wang, X. Dong, N. Zheng, H. Ma and X. Zhang, *Appl. Catal., B*, 2019, **257**, 117932.
63 Y. Zhao, Y. Zhao, R. Shi, B. Wang, G. I. N. Waterhouse, L.-Z. Wu, C.-H. Tung and T. Zhang, *Adv. Mater.*, 2019, **31**, 1806482.
64 X. Rong, H. Chen, J. Rong, X. Zhang, J. Wei, S. Liu, X. Zhou, J. Xu, F. Qiu and Z. Wu, *Chem. Eng. J.*, 2019, **371**, 286–293.
65 M. Song, M. Du, Q. Liu, F. Xing, C. Huang and X. Qiu, *Catal. Today*, 2019, **335**, 193–199.
66 X. Xue, R. Chen, C. Yan, Y. Hu, W. Zhang, S. Yang, L. Ma, G. Zhu and Z. Jin, *Nanoscale*, 2019, **11**, 10439–10445.
67 P. Guan, D. Xu, W. Fan and W. Shi, *Chem. Eng. J.*, 2019, **362**, 349–356.
68 N. Zhang, L. Li, Q. Shao, T. Zhu, X. Huang and X. Xiao, *ACS Appl. Energy Mater.*, 2019, **2**, 8394–8398.
69 T. Hou, R. Guo, L. Chen, Y. Xie, J. Guo, W. Zhang, X. Zheng, W. Zhu, X. Tan and L. Wang, *Nano Energy*, 2019, **65**, 104003.
70 X. Gao, Y. Shang, K. Gao and F. Fu, *Nanomaterials*, 2019, **9**, 781.
71 J. Fan, M. Zuo, Z. Ding, Z. Zhao, J. Liu and B. Sun, *Chem. Eng. J.*, 2020, **396**, 125263.
72 S. Wang, X. Hai, X. Ding, K. Chang, Y. Xiang, X. Meng, Z. Yang, H. Chen and J. Ye, *Adv. Mater.*, 2017, **29**, 1701774.
73 J. Di, J. Xia, M. F. Chisholm, J. Zhong, C. Chen, X. Cao, F. Dong, Z. Chi, H. Chen, Y.-X. Weng, J. Xiong, S.-Z. Yang, H. Li, Z. Liu and S. Dai, *Adv. Mater.*, 2019, **31**, 1807576.
74 G. Zhang, X. Yang, C. He, P. Zhang and H. Mi, *J. Mater. Chem. A*, 2020, **8**, 334–341.
75 Q. Liu, L. Ai and J. Jiang, *J. Mater. Chem. A*, 2018, **6**, 4102–4110.
76 X.-Y. Xie, P. Xiao, W.-H. Fang, G. Cui and W. Thiel, *ACS Catal.*, 2019, **9**, 9178–9187.
77 S. Wu, X. Tan, K. Liu, J. Lei, L. Wang and J. Zhang, *Catal. Today*, 2019, **335**, 214–220.
78 S. Sultana, S. Mansingh and K. M. Parida, *J. Mater. Chem. A*, 2019, **7**, 9145–9153.
79 X. Gao, Y. Shang, L. Liu and F. Fu, *J. Colloid Interface Sci.*, 2019, **533**, 649–657.
80 J. Yang, Y. Guo, R. Jiang, F. Qin, H. Zhang, W. Lu, J. Wang and J. C. Yu, *J. Am. Chem. Soc.*, 2018, **140**, 8497–8508.
81 G. Wu, L. Yu, Y. Liu, J. Zhao, Z. Han and G. Geng, *Appl. Surf. Sci.*, 2019, **481**, 649–660.
82 N. H. Kwon, S.-J. Shin, X. Jin, Y. Jung, G.-S. Hwang, H. Kim and S.-J. Hwang, *Appl. Catal., B*, 2020, **277**, 119191.
83 Y. Guo, J. Yang, D. Wu, H. Bai, Z. Yang, J. Wang and B. Yang, *J. Mater. Chem. A*, 2020, **8**, 16218–16231.
84 C. Ren, Y. Zhang, Y. Li, Y. Zhang, S. Huang, W. Lin and K. Ding, *J. Phys. Chem. C*, 2019, **123**, 17296–17305.
85 W. Wang, H. Zhang, S. Zhang, Y. Liu, G. Wang, C. Sun and H. Zhao, *Angew. Chem. Int. Ed.*, 2019, **58**, 16644–16650.
86 Y. Zhao, E. Wang and R. Jin, *Diamond Relat. Mater.*, 2019, **94**, 146–154.
87 T. Huang, S. Pan, L. Shi, A. Yu, X. Wang and Y. Fu, *Nanoscale*, 2020, **12**, 1833–1841.
88 Z. Li, G. Gu, S. Hu, X. Zou and G. Wu, *Chin. J. Catal.*, 2019, **40**, 1178–1186.
89 H. Wang, Y. Bu, G. Wu and X. Zou, *Dalton Trans.*, 2019, **48**, 11724–11731.
90 C. Liang, H.-Y. Niu, H. Guo, C.-G. Niu, D.-W. Huang, Y.-Y. Yang, H.-Y. Liu, B.-B. Shao and H.-P. Feng, *Chem. Eng. J.*, 2020, **396**, 125395.
91 C. Xiao, L. Zhang, K. Wang, H. Wang, Y. Zhou and W. Wang, *Appl. Catal., B*, 2018, **239**, 260–267.
92 X.-H. Li, W.-L. Chen, P. He, T. Wang, D. Liu, Y.-W. Li, Y.-G. Li and E.-B. Wang, *Inorg. Chem. Front.*, 2019, **6**, 3315–3326.
93 X. Hu, W. Zhang, Y. Yong, Y. Xu, X. Wang and X. Yao, *Appl. Surf. Sci.*, 2020, **510**, 145413.
94 Z. He, Y. Wang, X. Dong, N. Zheng, H. Ma and X. Zhang, *RSC Adv.*, 2019, **9**, 21646–21652.
95 X. Li, C. He, S. Zuo, X. Yan, D. Dai, Y. Zhang and C. Yao, *Sol. Energy*, 2019, **191**, 251–262.
96 H. Li, J. Li, Z. Ai, F. Jia and L. Zhang, *Angew. Chem. Int. Ed.*, 2018, **57**, 122–138.

97 T. Hou, H. Peng, Y. Xin, S. Wang, W. Zhu, L. Chen, Y. Yao, W. Zhang, S. Liang and L. Wang, *ACS Catal.*, 2020, **10**, 5502–5510.
98 C. Yao, R. Wang, Z. Wang, H. Lei, X. Dong and C. He, *J. Mater. Chem. A*, 2019, **7**, 27547–27559.
99 S. Liu, Y. Wang, S. Wang, M. You, S. Hong, T.-S. Wu, Y.-L. Soo, Z. Zhao, G. Jiang, J. Qiu, B. Wang and Z. Sun, *ACS Sustain. Chem. Eng.*, 2019, **7**, 6813–6820.
100 H. Huang, X.-S. Wang, D. Philo, F. Ichihara, H. Song, Y. Li, D. Li, T. Qiu, S. Wang and J. Ye, *Appl. Catal., B*, 2020, **267**, 118686.
101 A. Awati, H. Maimaiti, S. Wang and B. Xu, *Sci. Total Environ.*, 2019, **695**, 133865.
102 C. Hao, Y. Liao, Y. Wu, Y. An, J. Lin, Z. Gu, M. Jiang, S. Hu and X. Wang, *J. Phys. Chem. Solids*, 2020, **136**, 109141.
103 H. Liu, P. Wu, H. Li, Z. Chen, L. Wang, X. Zeng, Y. Zhu, Y. Jiang, X. Liao, B. S. Haynes, J. Ye, C. Stampfl and J. Huang, *Appl. Catal., B*, 2019, **259**, 118026.
104 T. Hou, L. Chen, Y. Xin, W. Zhu, C. Zhang, W. Zhang, S. Liang and L. Wang, *ACS Energy Lett.*, 2020, **5**, 2444–2451.
105 X. H. Li, W. L. Chen, H. Q. Tan, F. R. Li, J. P. Li, Y. G. Li and E. B. Wang, *ACS Appl. Mater. Interfaces*, 2019, **11**, 37927–37938.
106 K. Wang, G. Gu, S. Hu, J. Zhang, X. Sun, F. Wang, P. Li, Y. Zhao, Z. Fan and X. Zou, *Chem. Eng. J.*, 2019, **368**, 896–904.
107 H. Zhang, X. Li, H. Su, X. Chen, S. Zuo, X. Yan, W. Liu and C. Yao, *J. Sol-Gel Sci. Technol.*, 2019, **92**, 154–162.
108 G. Gu, K. Wang, N. Xiong, Z. Li, Z. Fan, S. Hu and X. Zou, *Dalton Trans.*, 2019, **48**, 5083–5089.
109 M. Nazemi and M. A. El-Sayed, *Nano Energy*, 2019, **63**, 103886.
110 C. Zhang, Y. Xu, C. Lv, X. Zhou, Y. Wang, W. Xing, Q. Meng, Y. Kong and G. Chen, *ACS Appl. Mater. Interfaces*, 2019, **11**, 29917–29923.
111 P. Xing, P. Chen, Z. Chen, X. Hu, H. Lin, Y. Wu, L. Zhao and Y. He, *ACS Sustainable Chem. Eng.*, 2018, **6**, 14866–14879.
112 X.-W. Guo, S.-M. Chen, H.-J. Wang, Z.-M. Zhang, H. Lin, L. Song and T.-B. Lu, *J. Mater. Chem. A*, 2019, **7**, 19831–19837.
113 P. Xing, S. Wu, Y. Chen, P. Chen, X. Hu, H. Lin, L. Zhao and Y. He, *ACS Sustainable Chem. Eng.*, 2019, **7**, 12408–12418.
114 L. Guo, X. Han, K. Zhang, Y. Zhang, Q. Zhao, D. Wang and F. Fu, *Catalysts*, 2019, **9**, 729.
115 J. Liu, R. Li, X. Zu, X. Zhang, Y. Wang, Y. Wang and C. Fan, *Chem. Eng. J.*, 2019, **371**, 796–803.
116 R. Zaffaroni, D. Ripepi, J. Middelkoop and F. M. Mulder, *ACS Energy Lett.*, 2020, **5**, 3773–3777.
117 Y. Zhao, R. Shi, X. Bian, C. Zhou, Y. Zhao, S. Zhang, F. Wu, G. I. N. Waterhouse, L.-Z. Wu, C.-H. Tung and T. Zhang, *Adv. Sci.*, 2019, **6**, 1802109.
118 Q. Meng, C. Lv, J. Sun, W. Hong, W. Xing, L. Qiang, G. Chen and X. Jin, *Appl. Catal., B*, 2019, **256**, 117781.